Second-order Decoupled Energy-stable Schemes for Cahn-Hilliard-Navier-Stokes equations

Jia Zhao[1,*] and Daozhi Han [2]

[1] *Department of Mathematics & Statistics, Utah State University, Logan, UT, USA;*
[2] *Department of Mathematics & Statistics, Missouri University of Science and Technology, Rolla, MO , USA.*

Abstract. The Cahn-Hilliard-Navier-Stokes (CHNS) equations represent the fundamental building blocks of hydrodynamic phase-field models for multiphase fluid flow dynamics. Due to the coupling between the Navier-Stokes equation and the Cahn-Hilliard equation, the CHNS system is non-trivial to solve numerically. Traditionally, a numerical extrapolation for the coupling terms is used. However, such brute-force extrapolation usually destroys the intrinsic thermodynamic structures of this CHNS system. This paper proposes a new strategy to reformulate the CHNS system into a constraint gradient flow formation. Under the new formulation, the reversible and irreversible structures are clearly revealed. This guides us to propose operator splitting schemes that have several advantageous properties. First of all, the proposed schemes lead to several decoupled systems in smaller sizes to be solved at each time marching step. This significantly reduces computational costs. Secondly, the proposed schemes still guarantee the thermodynamic laws of the CHNS system at the discrete level. In addition, unlike the recently populated IEQ or SAV approach using auxiliary variables, our resulting energy laws are formulated in the original variables. This is a significant improvement, as the modified energy laws with auxiliary variables sometimes deviate from the original energy law. Our proposed framework lays a foundation for designing decoupled and energy stable numerical algorithms for hydrodynamic phase-field models. Furthermore, various numerical algorithms can be obtained given different splitting steps, making this framework rather general. The proposed numerical algorithms are implemented. Their second-order temporal and spatial accuracy are verified numerically. Some numerical examples and benchmark problems are calculated to verify the effectiveness of the proposed schemes.

Key words: Phase Field; Decoupled Scheme; Energy Stable; Cahn-Hilliard-Navier-Srtokes; Hydrodynamics.

---

1 Background

Multiphase interfacial problems are ubiquitous in nature and industrial processes. As one of the most widely used approaches, phase field methods/models have been broadly utilized in various fields to investigate interfacial problems [1–3, 5, 10, 29, 33, 34, 47]. The phase-field method's major advantage is that the evolving interface is captured intrinsically instead of explicitly like other interface tracking methods. This dramatically simplifies the modeling and computational processes. Mainly, one needs to introduce phase-field variables that could either be the volume fractions or labels for the phases. Then continuous partial differential equations (PDEs) are proposed in the computational domain. Once the PDEs are solved, the interfaces will be retrieved through level sets of the phase variables. The phase-field models are also known as diffuse interface models since an artificial diffuse interface is usually introduced to regularize the phase variables, which are the PDEs' solutions [9]. Due to its simplicity in the theoretical formulation and numerical implementation, the phase-field method has been widely used in the fields where multiple material phases are involved [7, 24, 30, 40, 41, 50]. The velocity fields shall be considered when the material systems are fluids since the interactions between kinetics energy and free energy are not ignorable. Thus, the hydrodynamic equations for fluid flows will be proposed along with the phase-field equations for the phase variables. The well-known Cahn-Hilliard-Navier-Stokes equations are the fundamental system for the hydrodynamic phase-field

---

Corresponding author. Email address: `jia.zhao@usu.edu`. (J. Zhao) `handaoz@mst.edu`. (D. Han)

models [4,6,21,31]. It has been widely used to investigate interfacial problems for the incompressible fluid mixture.

Consider the domain Ω and time $t \in (0,T]$, and denote $\Omega_T = \Omega \times (0,T]$. In this paper, we use $\phi \in [-1,1]$ as the phase variable, with $\phi = 1$ to label one phase, $\phi = -1$ to label the other phase, and $\phi = 0$ representing the interface. The total energy of the two phase fluid-mixture system $\mathcal{E}$ include the Helmholtz free energy F and the kinetic energy E, i.e.

$$\mathcal{E}(\mathbf{u},\phi) = F(\phi) + E(\mathbf{u}), \quad F(\phi) = \int_\Omega \gamma \Big(\frac{\varepsilon}{2}|\nabla\phi|^2 + \frac{1}{\varepsilon}f(\phi)\Big)d\mathbf{x}, \quad E(\mathbf{u}) = \int_\Omega \frac{\rho}{2}|\mathbf{u}|^2 d\mathbf{x}. \tag{1.1}$$

where γ is the surface tension between the two fluid phases, ε is an artificial parameter controlling the interfacial thickness. $f(\phi)$ is the bulk free energy for the two phase material. $\mathbf{u}$ the volume-averaged velocity, and ρ is the volume-averaged density. In this paper, we assume the fluid mixture is incompressible, and both phases have the same density. The double-well potential

$$f(\phi) = \frac{1}{4}(\phi^2 - 1)^2 \tag{1.2}$$

will be used as the bulk potential in the rest of this paper. Other cases, such as the Flory-Huggins bulk potential [13,22], could be treated similarly with our proposed algorithms in this paper.

Then, the Cahn-Hilliard-Navier-Stokes (CHNS) equations are formulated as [4,6,21,31]

$$\begin{cases} \rho\Big(\partial_t\mathbf{u} + \mathbf{u}\cdot\nabla\mathbf{u}\Big) = -\nabla p + \eta\nabla^2\mathbf{u} - \phi\nabla\mu, \quad (\mathbf{x},t) \in \Omega_T, \\ \nabla\cdot\mathbf{u} = 0, \quad (\mathbf{x},t) \in \Omega_T, \\ \partial_t\phi + \nabla\cdot(\mathbf{u}\phi) = \nabla\cdot(M(\phi)\nabla\mu), \quad (\mathbf{x},t) \in \Omega_T, \\ \mu = -\gamma\varepsilon\Delta\phi + \frac{\gamma}{\varepsilon}f'(\phi), \quad (\mathbf{x},t) \in \Omega_T, \end{cases} \tag{1.3}$$

where η is the viscosity parameter, $M(\phi) \geq 0$ is the mobility operator, p is the hydrodynamic pressure, and $\mu = \frac{\delta F}{\delta\phi}$ is the chemical potential. The boundary conditions are not unique. In this paper, if not otherwise specified, we focus on the following physical boundary conditions:

$$\mathbf{u}(\mathbf{x},t) = 0, \quad \nabla\mu(\mathbf{x},t)\cdot\mathbf{n} = 0, \quad \nabla\phi(\mathbf{x},t)\cdot\mathbf{n} = 0, \quad (\mathbf{x},t) \in \partial\Omega \times (0,T], \tag{1.4}$$

with $\mathbf{n}$ the outward normal vector at the boundary. The CHNS system in (1.3)-(1.4) is known to satisfy the second law of thermodynamics [4,6,21,31], with the energy dissipation rate calculated as

$$\frac{d\mathcal{E}}{dt} = -\int_\Omega \Big(|\sqrt{M(\phi)}\nabla\mu|^2 + \eta|\nabla\mathbf{u}|^2\Big)d\mathbf{x}. \tag{1.5}$$

One principle in developing numerical algorithms for solving the CHNS system is to guarantee that the numerical solutions also satisfy the energy law in (1.5). A numerical scheme that satisfies the monotone property of the energy is known as an energy stable scheme or energy-law-preserving scheme [11]. In an energy-stable scheme, the energy of the system remains bounded (non-increasing) at any time step regardless of the time step size, cf. (1.5). Therefore energy-stable schemes allow large time marching while preserving accuracy and stability, which is essential in solving stiff systems such as the CHNS system [35].

Given the significant role it played in the phase-field models, the CHNS system has drawn a considerable amount of attention. Many seminal works have been published investigating different aspects. Here we briefly review some relevant results in numerical analysis. There are several pieces of existing works on fully discrete schemes for the hydrodynamic phase-field model or its simplified versions [8,20,21,42], all of them are either only first-order in time or nonlinear. In comparison, our decoupled schemes can be more efficient in implementation and computational costs. Han and Wang introduce a second-order velocity projection method for the CHNS system in [21]. The resulted numerical scheme is second-order accurate in time. This is one of the earliest works to introduce second-order numerical algorithms for the CHNS system while preserving energy stability. Later Gong et al.

manage to improve the scheme by using the energy quadratization (EQ) idea, such that only linear systems need to be solved at each time step [15]. Another linear and energy stable scheme is introduced in [6], where a stabilized leap-frog type time-marching strategy is adapted. However, the velocity field and phase variables have to be solved simultaneously in all the schemes just mentioned. This requires either a Newton iteration method or a fixed-point iteration method. This drawback shall not be ignored since the solution's existence, and uniqueness for the iteration method usually have substantial requirements on the time step, making the unconditional stability of the original numerical algorithms less appealing. We also note that some second-order (linear) energy stable schemes have been developed for thermodynamic phase-field equations in recent years [12,14,18,26,37], which may potentially be applicable to hydrodynamic phase-field models.

Due to the coupling between the hydrodynamic equation and the phase-field equation, it is desirable to develop accurate and efficient numerical algorithms that can decouple the two equations. It is preferred that, in each time marching step, only a smaller size of problems shall be solved sequentially. This is the primary motivation of this paper. Seeking decoupled numerical algorithms that can solve the velocity field $\mathbf{u}$ and phase variable ϕ independently has been an active research topic. One approach is to treat the velocity $\mathbf{u}$ explicitly in the Cahn-Hilliard equation, cf. [23,28]. As is shown in [23], the energy law is preserved under a CFL condition. Minjeaud realized that a first-order relaxation on the velocity field could uncouple the velocity field and phase variable such that decoupled numerical algorithms for triphasic Cahn-Hilliard-Navier-Stoke model can be developed [31]. This idea has been further populated to investigate various hydrodynamic phase field models [25,38,46,49], for which one can get a linearly decoupled scheme such that the velocity field, phase variable, and pressure can be solved sequentially. Each of the sub-problems is an elliptic-type equation so that fast and efficient solvers can be applied. But due to the unavoidable first-order modification on the velocity field, the accuracy is restricted to first-order, which is not much attractive for practical application. In parallel, the idea of the scalar auxiliary variable (SAV) has been used to decouple the phase field and hydrodynamic systems [27,44], from which second-order decoupled schemes could be developed. However, such strategies usually introduce new variables so that discrete energy laws are modified using the auxiliary variables, making the connections with the energy law with original variables less clear.

In this paper, we come up with a novel approach to overcome all these difficulties mentioned above. Mainly, we propose an elegant strategy to develop decoupled and energy stable numerical algorithms for the CHNS system in a confined geometry subject to physical boundary conditions. We first reformulate the CHNS system into a constraint gradient flow system. This reformulation provides insights into the numerical algorithm design. With the constraint gradient flow formation, we propose several variants of second-order operator splitting schemes. All the schemes uncouple the velocity field and phase variables so that only smaller systems need to be solved in each time marching step. Besides the efficiency, all the schemes are rigorously shown to be energy stable, i.e., satisfy the discrete energy law. We emphasize that our proposed schemes hold the discrete energy laws in the original variables, which differs from the EQ or SAV approaches [37,45].

The rest of the paper is organized as follows. We first reformulate the CHNS system into a constraint gradient flow formulation in Section 2. Then we discretize the space with a second-order finite difference on staggered grids in Section 3. Afterward, we introduce the second-order splitting techniques to design second-order accurate in time and decoupled numerical algorithms for solving the CHNS system in Section 4. The energy stable property of the proposed schemes is also rigorously proved. Then, in Section 5, we present the convergence tests and several benchmark problems. The numerical results highlight the effectiveness of our proposed decoupled numerical schemes. In the end, we give a brief conclusion.

2   Model Reformulation of CHNS equations

2.1   Some notations

First of all, we illustrate the reformation of the incompressible CHNS system. Notice the pressure p in (1.3) is a Lagrangian multiplier to enforce the in-compressibility of the velocity field $\mathbf{u}$. With this in mind, we can reformulate the CHNS system into a constraint gradient flow form that will guide us

in designing decoupled numerical algorithms.

Consider a regular domain Ω in d dimension. For any $f,g \in [L^2(\Omega)]^d$, we denote the inner product and induced L^2 norm as

$$(f,g) = \int_\Omega \sum_{i=1}^d f_i g_i d\mathbf{x}, \quad \|f\| = \sqrt{(f,f)}. \tag{2.1}$$

Follow the notations in [17,32]. Let $P_\mathbf{u}$ be a functional space defined by

$$P_\mathbf{u} = \left\{ \mathbf{u}(\mathbf{x},t) : \mathbf{u} \in [L^2(\Omega)]^d; \quad \nabla \cdot \mathbf{u} = 0 \text{ in } \Omega, \quad \mathbf{u} = 0 \text{ on } \partial\Omega \right\}. \tag{2.2}$$

The divergence free projection operator $\Pi_\mathbf{u} : [L^2(\Omega)]^d \to P_\mathbf{u}$ is defined as

$$\Pi_\mathbf{u}(\mathbf{a}) = \begin{cases} \mathbf{a} - \nabla p, & \text{in } \Omega/\partial\Omega, \\ 0 & \text{on } \partial\Omega, \end{cases} \tag{2.3}$$

where p satisfies a Poisson equation with a Neumann-type boundary condition, as shown below

$$\begin{cases} \Delta p = \nabla \cdot \mathbf{a}, & \text{in } \Omega, \\ \frac{\partial p}{\partial \mathbf{n}} = \mathbf{a} \cdot \mathbf{n}, & \text{on } \partial\Omega. \end{cases}$$

With the projection operator $\Pi_\mathbf{u}$ in (2.3), we denote the constraint variational derivative of the kinetic energy E in (1.1) with respect to the velocity field as

$$\frac{\delta E}{\delta \mathbf{u}} = \Pi_\mathbf{u} \frac{\partial E}{\partial \mathbf{u}}. \tag{2.4}$$

Next, we illustrate the reformulation of the convection term in the Navier-Stokes equation. We introduce the skew-symmetric form for the nonlinear convection term as

$$B(\mathbf{v},\mathbf{u}) = \frac{1}{2} \left[\mathbf{v} \cdot \nabla \mathbf{u} + \nabla \cdot (\mathbf{v}\mathbf{u}) \right]. \tag{2.5}$$

It induces a trilinear form b defined as [21]

$$b(\mathbf{v},\mathbf{u},\mathbf{w}) = \left(B(\mathbf{v},\mathbf{u}),\mathbf{w} \right) = \frac{1}{2} \left[\left(\mathbf{v} \cdot \nabla \mathbf{u},\mathbf{w} \right) - \left(\mathbf{v} \cdot \nabla \mathbf{w},\mathbf{u} \right) \right], \quad \forall \mathbf{u},\mathbf{v},\mathbf{w} \in \mathbf{H}_0^1(\Omega), \tag{2.6}$$

which has the property $b(\mathbf{v},\mathbf{u},\mathbf{u}) = 0$, $\forall \mathbf{u},\mathbf{v} \in \mathbf{H}_0^1(\Omega)$.

Remark 2.1. The reformulation of the skew-symmetric form $B(\mathbf{v},\mathbf{u})$ for the convection term is not unique. An alternative skew-symmetric form is $B(\mathbf{v},\mathbf{u}) = (\mathbf{v} \cdot \nabla)\mathbf{u} + \frac{1}{2}(\nabla \cdot \mathbf{v})\mathbf{u}$.

2.2 Model reformulation

Given $\nabla \cdot \mathbf{u} = 0$, we have the property $B(\mathbf{u},\mathbf{u}) = \mathbf{u} \cdot \nabla \mathbf{u}$. The incompressible CHNS system in (1.3) can be rewritten as

$$\rho(\partial_t \mathbf{u} + B(\mathbf{u},\mathbf{u})) = -\nabla p + \eta \Delta \mathbf{u} - \phi \nabla \mu. \tag{2.7}$$

With the constraint variation in (2.4) and reformulation of the convection term in (2.5), we rewrite the CHNS equation in (1.3) as a constraint gradient flow form

$$\Lambda \partial_t \Psi = \mathcal{G} \frac{\delta \mathcal{E}}{\delta \Psi}, \quad \Lambda = \begin{bmatrix} \rho & 0 \\ 0 & 1 \end{bmatrix}, \quad \Psi = \begin{bmatrix} \mathbf{u} \\ \phi \end{bmatrix}, \quad \mathcal{G} = \begin{pmatrix} \beta \Delta \bullet - B(\mathbf{u},\bullet) & -\phi \nabla \bullet \\ -\nabla \cdot (\bullet \phi) & \nabla \cdot (M(\phi)\nabla \bullet) \end{pmatrix}, \tag{2.8}$$

with proper boundary conditions and initial values. Here $\frac{\delta \mathcal{E}}{\delta \mathbf{u}} := \Pi_\mathbf{u} \frac{\partial E}{\partial \mathbf{u}}$ is defined using the projection operator as shown in (2.4). $\mathcal{G}$ is called the mobility operator.

Remark 2.2. This constraint gradient flow reformulation is not limited to the Cahn-Hilliard-Navier-Stokes system. Other thermodynamic consistent hydrodynamic models could be reformulated similarly. We will not elaborate on it due to space limitations.

2.3 Splitting strategies for the mobility operator $\mathcal{G}$

The mobility operator $\mathcal{G}$ can be splitting as two parts: $\mathcal{G}:=\mathcal{G}_a+\mathcal{G}_s$. One splitting instance is defined as

$$\mathcal{G}_a=\begin{pmatrix} 0 & -\phi\nabla\bullet \\ -\nabla\cdot(\bullet\phi) & 0 \end{pmatrix}, \quad \mathcal{G}_s=\begin{pmatrix} \eta\Delta\bullet-B(\mathbf{u},\bullet) & 0 \\ 0 & \nabla\cdot(M(\phi)\nabla\bullet) \end{pmatrix}. \tag{2.9}$$

Here $\mathcal{G}_a$ controls the reversible dynamics, representing the energy exchanges between the kinetic energy and the Helmholtz free energy, and $\mathcal{G}_s$ controls the irreversible dynamics, representing the energy dissipation.

The splitting of the mobility operator $\mathcal{G}=\mathcal{G}_a+\mathcal{G}_s$ is not unique. Different splitting strategies will lead to different numerical algorithms, which will be elaborated in later sections. In particular, we introduce an alternative splitting as below

$$\mathcal{G}_a=\begin{pmatrix} 0 & -\phi\nabla\bullet \\ -\nabla\cdot(\bullet\phi) & \nabla\cdot(M(\phi)\nabla\bullet) \end{pmatrix}, \quad \mathcal{G}_s=\begin{pmatrix} \eta\Delta\bullet-B(\mathbf{u},\bullet) & 0 \\ 0 & 0 \end{pmatrix}. \tag{2.10}$$

3 Spatial Discretization on Staggered Grids

In this section, we present the spatial discretization of the CHNS system in (1.3) with physical boundary conditions in (1.4).

3.1 Notations for spatial discretization

To simplify the presentation, we introduce some finite difference notations for spatial discretization. Although these notations can also be found in [8,15,36,42,43], we summarize them in this section to make this paper reader-friendly.

We consider a rectangular spatial domain $\Omega=[0,L_x]\times[0,L_y]$ with L_x and L_y two positive numbers. The domain is discretized into uniform rectangular meshes with mesh size $h_x=\frac{L_x}{N_x}$ and $h_y=\frac{L_y}{N_y}$. Here N_x and N_y are two positive integers. We define the following 1D sets for grid points

$$E_x=\{x_{i+\frac{1}{2}}|i=0,1,\dots,N_x\}, \quad C_x=\{x_i|i=1,2,\dots,N_x\}, \quad C_{\overline{x}}=\{x_i|i=0,1,\dots,N_x+1\},$$
$$E_y=\{y_{j+\frac{1}{2}}|j=0,1,\dots,N_y\}, \quad C_y=\{y_j|j=1,2,\dots,N_y\}, \quad C_{\overline{y}}=\{y_j|j=0,1,\dots,N_y+1\},$$

where $x_l=(l-\frac{1}{2})h_x$, $y_l=(l-\frac{1}{2})h_y$, and l can take on either integer or half-integer values. E_x is called a uniform partition of $[0,L_x]$ of size N_x, and its elements are called edge-centered points. The elements of C_x and $C_{\overline{x}}$ are called cell-centered points. The two points belonging to $C_{\overline{x}}\backslash C_x$ are called ghost points. Analogously, the set E_y is a uniform partition of $[0,L_y]$ of size N_y, called edge-centered points, and C_y and $C_{\overline{y}}$ contain the cell-centered points of the interval $[0,L_y]$.

We define the following discrete function spaces

$$\mathcal{C}_{x\times y}=\{\phi:C_x\times C_y\to\mathbb{R}\}, \quad \mathcal{C}_{\overline{x}\times y}=\{\phi:C_{\overline{x}}\times C_y\to\mathbb{R}\}, \quad \mathcal{C}_{x\times\overline{y}}=\{\phi:C_x\times C_{\overline{y}}\to\mathbb{R}\},$$
$$\mathcal{C}_{\overline{x}\times\overline{y}}=\{\phi:C_{\overline{x}}\times C_{\overline{y}}\to\mathbb{R}\}, \quad \mathcal{E}^{ew}_{x\times y}=\{u:E_x\times C_y\to\mathbb{R}\}, \quad \mathcal{E}^{ew}_{x\times\overline{y}}=\{u:E_x\times C_{\overline{y}}\to\mathbb{R}\},$$
$$\mathcal{E}^{ns}_{x\times y}=\{v:C_x\times E_y\to\mathbb{R}\}, \quad \mathcal{E}^{ns}_{\overline{x}\times y}=\{v:C_{\overline{x}}\times E_y\to\mathbb{R}\}, \quad \mathcal{V}_{x\times y}=\{f:E_x\times E_y\to\mathbb{R}\}.$$

Throughout this paper, we denote the cell-centered, edge-centered and vertex-centered discrete functions as follows:

$$\begin{aligned} \text{cell centered functions:} \quad & \phi,\psi,\mu\in\mathcal{C}_{x\times y}\cup\mathcal{C}_{\overline{x}\times y}\cup\mathcal{C}_{x\times\overline{y}}\cup\mathcal{C}_{\overline{x}\times\overline{y}}, \\ \text{east west edge centered functions:} \quad & u,r\in\mathcal{E}^{ew}_{x\times y}\cup\mathcal{E}^{ew}_{x\times\overline{y}}, \\ \text{north south edge centered functions:} \quad & v,w\in\mathcal{E}^{ns}_{x\times y}\cup\mathcal{E}^{ns}_{\overline{x}\times y}, \\ \text{vertex centered functions:} \quad & f,g\in\mathcal{V}_{x\times y}. \end{aligned}$$

We define the discrete function spaces with homogeneous Dirichlet boundary conditions as follows:

$$\mathcal{E}_{x \times y}^{ew0} = \{u \in \mathcal{E}_{x \times y}^{ew} \cup \mathcal{E}_{x \times \overline{y}}^{ew} | u_{\frac{1}{2},j} = u_{N_x+\frac{1}{2},j} = 0, \ j = 1,2,...,N_y\},$$

$$\mathcal{E}_{x \times \overline{y}}^{ew0} = \{u \in \mathcal{E}_{x \times \overline{y}}^{ew} | u_{\frac{1}{2},j} = u_{N_x+\frac{1}{2},j} = 0, \ j = 0,1,...,N_y+1\},$$

$$\mathcal{E}_{x \times y}^{ns0} = \{v \in \mathcal{E}_{x \times y}^{ns} \cup \mathcal{E}_{\overline{x} \times y}^{ns} | v_{i,\frac{1}{2}} = v_{i,N_y+\frac{1}{2}} = 0, \ i = 1,2,...,N_x\},$$

$$\mathcal{E}_{\overline{x} \times y}^{ns0} = \{v \in \mathcal{E}_{\overline{x} \times y}^{ns} | v_{i,\frac{1}{2}} = v_{i,N_y+\frac{1}{2}} = 0, \ i = 0,1,...,N_x+1\},$$

$$\mathcal{V}_{x \times y}^{ew0} = \{f \in \mathcal{V}_{x \times y} | f_{\frac{1}{2},j+\frac{1}{2}} = f_{N_x+\frac{1}{2},j+\frac{1}{2}} = 0, \ j = 0,1,...,N_y\},$$

$$\mathcal{V}_{x \times y}^{ns0} = \{f \in \mathcal{V}_{x \times y} | f_{i+\frac{1}{2},\frac{1}{2}} = f_{i+\frac{1}{2},N_y+\frac{1}{2}} = 0, \ i = 0,1,...,N_x\},$$

$$\mathcal{V}_{x \times y}^{0} = \mathcal{V}_{x \times y}^{ew0} \cap \mathcal{V}_{x \times y}^{ns0}.$$

Note that $\mathcal{E}_{x \times \overline{y}}^{ew0} \subset \mathcal{E}_{x \times y}^{ew0}$ and $\mathcal{E}_{\overline{x} \times y}^{ns0} \subset \mathcal{E}_{x \times y}^{ns0}$. The east-west-edge-to-center average and difference operators are defined as $a_x, d_x : \mathcal{E}_{x \times \overline{y}}^{ew} \cup \mathcal{V}_{x \times y} \to \mathcal{C}_{x \times \overline{y}} \cup \mathcal{E}_{x \times y}^{ns}$ in component-wise forms:

$$a_x u_{i,j} = \frac{1}{2}(u_{i+\frac{1}{2},j} + u_{i-\frac{1}{2},j}), \quad d_x u_{i,j} = \frac{1}{h_x}(u_{i+\frac{1}{2},j} - u_{i-\frac{1}{2},j}), \quad a_x u, d_x u \in \mathcal{C}_{x \times \overline{y}},$$

$$a_x f_{i,j+\frac{1}{2}} = \frac{1}{2}(f_{i+\frac{1}{2},j+\frac{1}{2}} + f_{i-\frac{1}{2},j+\frac{1}{2}}), \quad d_x f_{i,j+\frac{1}{2}} = \frac{1}{h_x}(f_{i+\frac{1}{2},j+\frac{1}{2}} - f_{i-\frac{1}{2},j+\frac{1}{2}}), \quad a_x f, d_x f \in \mathcal{E}_{x \times y}^{ns}.$$

The north-south-edge-to-center average and difference operators are defined as $a_y, d_y : \mathcal{E}_{\overline{x} \times y}^{ns} \cup \mathcal{V}_{x \times y} \to \mathcal{C}_{\overline{x} \times y} \cup \mathcal{E}_{x \times y}^{ew}$ in component-wise forms:

$$a_y v_{i,j} = \frac{1}{2}(v_{i,j+\frac{1}{2}} + v_{i,j-\frac{1}{2}}), \quad d_y v_{i,j} = \frac{1}{h_y}(v_{i,j+\frac{1}{2}} - v_{i,j-\frac{1}{2}}), \quad a_y v, d_y v \in \mathcal{C}_{\overline{x} \times y},$$

$$a_y f_{i+\frac{1}{2},j} = \frac{1}{2}(f_{i+\frac{1}{2},j+\frac{1}{2}} + f_{i+\frac{1}{2},j-\frac{1}{2}}), \quad d_y f_{i+\frac{1}{2},j} = \frac{1}{h_y}(f_{i+\frac{1}{2},j+\frac{1}{2}} - f_{i+\frac{1}{2},j-\frac{1}{2}}), \quad a_y f, d_y f \in \mathcal{E}_{x \times y}^{ew}.$$

The center-to-east-west-edge average and difference operators are defined as $A_x, D_x : \mathcal{C}_{\overline{x} \times \overline{y}} \cup \mathcal{E}_{\overline{x} \times y}^{ns} \to \mathcal{E}_{x \times \overline{y}}^{ew} \cup \mathcal{V}_{x \times y}$ in component-wise forms:

$$A_x \phi_{i+\frac{1}{2},j} = \frac{1}{2}(\phi_{i+1,j} + \phi_{i,j}), \quad D_x \phi_{i+\frac{1}{2},j} = \frac{1}{h_x}(\phi_{i+1,j} - \phi_{i,j}), \quad A_x \phi, D_x \phi \in \mathcal{E}_{x \times \overline{y}}^{ew},$$

$$A_x v_{i+\frac{1}{2},j+\frac{1}{2}} = \frac{1}{2}(v_{i+1,j+\frac{1}{2}} + v_{i,j+\frac{1}{2}}), \quad D_x v_{i+\frac{1}{2},j+\frac{1}{2}} = \frac{1}{h_x}(v_{i+1,j+\frac{1}{2}} - v_{i,j+\frac{1}{2}}), \quad A_x v, D_x v \in \mathcal{V}_{x \times y}.$$

The center-to-north-south-edge average and difference operators are defined as $A_y, D_y : \mathcal{C}_{\overline{x} \times \overline{y}} \cup \mathcal{E}_{x \times \overline{y}}^{ew} \to \mathcal{E}_{\overline{x} \times y}^{ns} \cup \mathcal{V}_{x \times y}$ in component-wise forms:

$$A_y \phi_{i,j+\frac{1}{2}} = \frac{1}{2}(\phi_{i,j+1} + \phi_{i,j}), \quad D_y \phi_{i,j+\frac{1}{2}} = \frac{1}{h_y}(\phi_{i,j+1} - \phi_{i,j}), \quad A_y \phi, D_y \phi \in \mathcal{E}_{\overline{x} \times y}^{ns},$$

$$A_y u_{i+\frac{1}{2},j+\frac{1}{2}} = \frac{1}{2}(u_{i+\frac{1}{2},j+1} + u_{i+\frac{1}{2},j}), \quad D_y u_{i+\frac{1}{2},j+\frac{1}{2}} = \frac{1}{h_y}(u_{i+\frac{1}{2},j+1} - u_{i+\frac{1}{2},j}), \quad A_y u, D_y u \in \mathcal{V}_{x \times y}.$$

The discrete Laplacian operator $\Delta_h : \mathcal{C}_{\overline{x} \times \overline{y}} \to \mathcal{C}_{x \times y}$ is defined as

$$\Delta_h \phi = d_x(D_x \phi) + d_y(D_y \phi).$$

We discretize the physical variables that satisfy Neumann boundary conditions at the cell-center and the ones that satisfy Dirichlet boundary conditions at the edge-center. So, the cell-centered functions $\phi, \mu \in \mathcal{C}_{\overline{x} \times \overline{y}}$ satisfy homogeneous Neumann boundary conditions if and only if

$$\phi_{0,j} = \phi_{1,j}, \quad \phi_{N_x,j} = \phi_{N_x+1,j}, \quad \mu_{0,j} = \mu_{1,j}, \quad \mu_{N_x,j} = \mu_{N_x+1,j}, \quad j = 1,2,...,N_y, \tag{3.1}$$

$$\phi_{i,0} = \phi_{i,1}, \quad \phi_{i,N_y} = \phi_{i,N_y+1}, \quad \mu_{i,0} = \mu_{i,1}, \quad \mu_{i,N_y} = \mu_{i,N_y+1}, \quad i = 0,1,...,N_x+1. \tag{3.2}$$

The velocity $\mathbf{u}=(u,v)$ (for $u\in\mathcal{E}^{ew}_{x\times\overline{y}}$, $v\in\mathcal{E}^{ns}_{\overline{x}\times y}$) satisfies the no-slip (Dirichlet) boundary conditions $\mathbf{u}|_\Omega=0$ if and only if

$$u_{\frac{1}{2},j}=u_{N_x+\frac{1}{2},j}=0, \qquad j=1,2,\ldots,N_y, \tag{3.3}$$

$$A_y u_{i+\frac{1}{2},\frac{1}{2}}=A_y u_{i+\frac{1}{2},N_y+\frac{1}{2}}=0, \qquad i=0,1,\ldots,N_x, \tag{3.4}$$

$$v_{i,\frac{1}{2}}=v_{i,N_y+\frac{1}{2}}=0, \qquad i=1,2,\ldots,N_x, \tag{3.5}$$

$$A_x v_{\frac{1}{2},j+\frac{1}{2}}=A_x v_{N_x+\frac{1}{2},j+\frac{1}{2}}=0, \qquad j=0,1,\ldots,N_y. \tag{3.6}$$

It is easy to show that

$$D_x\phi,D_x\mu,u\in\mathcal{E}^{ew0}_{x\times\overline{y}}, \; D_y\phi,D_y\mu,v\in\mathcal{E}^{ns0}_{\overline{x}\times y}, \; A_yu,A_xv\in\mathcal{V}^0_{x\times y}, \; D_yu\in\mathcal{V}^{ew0}_{x\times y}, \; D_xv\in\mathcal{V}^{ns0}_{x\times y}. \tag{3.7}$$

Based on the above definitions, we define the following discrete 2D weighted inner-products:

$$(\phi,\psi)_2=h_x h_y\sum_{i=1}^{N_x}\sum_{j=1}^{N_y}\phi_{i,j}\psi_{i,j},$$

$$[u,r]_{ew}=(a_x(ur),1)_2, \quad [v,w]_{ns}=(a_y(vw),1)_2, \quad \langle f,g\rangle_{vc}=\big(a_x(a_y(fg)),1\big)_2,$$

and the corresponding discrete norms:

$$\|\phi\|_2=(\phi,\phi)_2^{\frac{1}{2}}, \quad \|u\|_{ew}=[u,u]_{ew}^{\frac{1}{2}}, \quad \|v\|_{ns}=[v,v]_{ns}^{\frac{1}{2}}, \quad \|f\|_{vc}=\langle f,f\rangle_{vc}^{\frac{1}{2}}.$$

Specially, we have

$$[u,r]_{ew}=h_x h_y\sum_{i=1}^{N_x-1}\sum_{j=1}^{N_y}u_{i+\frac{1}{2},j}r_{i+\frac{1}{2},j}, \text{ if } u\in\mathcal{E}^{ew0}_{x\times y},$$

$$[v,w]_{ns}=h_x h_y\sum_{i=1}^{N_x}\sum_{j=1}^{N_y-1}v_{i,j+\frac{1}{2}}w_{i,j+\frac{1}{2}}, \text{ if } v\in\mathcal{E}^{ns0}_{x\times y},$$

$$\langle f,g\rangle_{vc}=h_x h_y\sum_{i=1}^{N_x-1}\sum_{j=1}^{N_y-1}f_{i+\frac{1}{2},j+\frac{1}{2}}g_{i+\frac{1}{2},j+\frac{1}{2}}, \text{ if } f\in\mathcal{V}^0_{x\times y}.$$

For the edge-centered function $\mathbf{u}=(u,v)$, $u\in\mathcal{E}^{ew}_{x\times\overline{y}}, v\in\mathcal{E}^{ns}_{\overline{x}\times y}$ and the cell-centered function $\phi\in\mathcal{C}_{\overline{x}\times\overline{y}}$, we define the following norms

$$\|\mathbf{u}\|_2:=\sqrt{\|u\|^2_{ew}+\|v\|^2_{ns}}, \quad \|\nabla\phi\|_2:=\sqrt{\|D_x\phi\|^2_{ew}+\|D_y\phi\|^2_{ns}}.$$

Next, we introduce some useful lemmas [15].

Lemma 3.1. *For $\phi\in\mathcal{C}_{\overline{x}\times\overline{y}}$, $u\in\mathcal{E}^{ew0}_{x\times y}$, $v\in\mathcal{E}^{ns0}_{x\times y}$, there exist the following identities:*

$$[A_x\phi,u]_{ew}=(\phi,a_xu)_2, \quad [D_x\phi,u]_{ew}+(\phi,d_xu)_2=0, \tag{3.8}$$

$$[A_y\phi,v]_{ns}=(\phi,a_yv)_2, \quad [D_y\phi,v]_{ns}+(\phi,d_yv)_2=0. \tag{3.9}$$

Lemma 3.2. *For $f\in\mathcal{V}^0_{x\times y}$, $u\in\mathcal{E}^{ew}_{x\times\overline{y}}$, $v\in\mathcal{E}^{ns}_{\overline{x}\times y}$, there exists the identities:*

$$\langle f,A_yu\rangle_{vc}=[a_yf,u]_{ew}, \quad \langle f,D_yu\rangle_{vc}+[d_yf,u]_{ew}=0, \tag{3.10}$$

$$\langle f,A_xv\rangle_{vc}=[a_xf,v]_{ns}, \quad \langle f,D_xv\rangle_{vc}+[d_xf,v]_{ns}=0. \tag{3.11}$$

Lemma 3.3. *For $f\in\mathcal{V}_{x\times y}$, $u\in\mathcal{E}^{ew}_{x\times\overline{y}}$, $v\in\mathcal{E}^{ns}_{\overline{x}\times y}$ and $A_yu,A_xv\in\mathcal{V}^0_{x\times y}$, there exist the identities:*

$$\langle f,D_yu\rangle_{vc}+[d_yf,u]_{ew}=0, \tag{3.12}$$

$$\langle f,D_xv\rangle_{vc}+[d_xf,v]_{ns}=0. \tag{3.13}$$

3.2 Spatial discretization

With the notation above, we are ready to explain the spatial discretization of the CHNS on staggered grids. To write it in a clear manner, we write the spatial discretization in the following component form

$$\rho\partial_t u+\frac{\rho}{2}\Big(u\partial_x u+\partial_x(uu)+v\partial_y u+\partial_y(vu)\Big)=-\partial_x p+\eta\partial_x\partial_x u-\phi\partial_x\mu, \tag{3.14a}$$

$$\rho\partial_t v+\frac{\rho}{2}\Big(u\partial_x v+\partial_x(uv)+v\partial_y v+\partial_y(vv)\Big)=-\partial_y p+\eta\partial_y\partial_y v-\phi\partial_y\mu, \tag{3.14b}$$

$$\partial_x u+\partial_y v=0, \tag{3.14c}$$

$$\partial_t\phi+\partial_x(\phi u)+\partial_y(\phi v)=\partial_x\Big(M(\phi)\partial_x\mu\Big)+\partial_y\Big(M(\phi)\partial_y\mu\Big), \tag{3.14d}$$

$$\mu=-\gamma\varepsilon\Delta\phi+\frac{\gamma}{\varepsilon}f'(\phi), \tag{3.14e}$$

where $\mathbf{u}=(u,v)$. Then, we apply the finite difference spatial discretization on a staggered grid on the system (3.14).

Scheme 3.1 (Semi-discrete Scheme). Applying staggered-grid finite differences in space to the system (3.14) with boundary conditions (1.4), we obtain a semi-discrete scheme as follows:

$$\Big\{\rho\frac{d}{dt}u+\frac{\rho}{2}\Big(uD_x(a_x u)+A_x\big(d_x(uu)\big)+a_y(A_x vD_y u)+d_y(A_y uA_x v)\Big)$$
$$=-D_x p+\eta D_x d_x u-A_x\phi D_x\mu\Big\}_{i+\frac{1}{2},j}, \tag{3.15a}$$

$$\Big\{\rho\frac{d}{dt}v+\frac{\rho}{2}\Big(a_x(A_y uD_x v)+d_x\big(A_y uA_x v\big)+vD_y(a_y v)+A_y\big(d_y(vv)\big)\Big)$$
$$=-D_y p++\eta D_y d_y v-A_y\phi D_y\mu\Big\}_{i,j+\frac{1}{2}}, \tag{3.15b}$$

$$\Big\{d_x u+d_y v=0\Big\}_{i,j}, \tag{3.15c}$$

$$\Big\{\frac{d}{dt}\phi+d_x(A_x\phi u)+d_y(A_y\phi v)=d_x\big(M(A_x\phi)D_x\mu\big)+d_y\big(M(A_y\phi)D_y\mu\big)\Big\}_{i,j}, \tag{3.15d}$$

$$\Big\{\mu=-\gamma\varepsilon\Delta_h\phi+\frac{\gamma}{\varepsilon}f'(\phi)\Big\}_{i,j}, \tag{3.15e}$$

where u,v,ϕ,μ satisfy the discrete boundary conditions (3.1)-(3.6), and $i=1,\dots,N_x-1,j=1,\dots,N_y$ for Eq. (3.15a), $i=1,\dots,N_x,j=1,\dots,N_y-1$ for Eq. (3.15b), $i=1,\dots,N_x,j=1,\dots,N_y$ for Eqs. (3.15c)-(3.15e).

We can easily show that the semi-discrete scheme 3.1 has the following two properties.

Theorem 3.1. *The semi-discrete scheme 3.1 preserves the discrete mass conservation law given by*

$$\frac{d}{dt}(\phi,1)_2=0. \tag{3.16}$$

Proof. This can be easily verified. In fact, we can compute the discrete inner product of (3.15d) with constant function 1, and use (3.7) and Lemma 3.1. Then, this leads us to (3.16). □

Theorem 3.2. *The semi-discrete scheme 3.1 preserves the discrete energy dissipation law*

$$\frac{d}{dt}E_h+\Big(\eta,(d_x u)^2+(d_y v)^2\Big)_2+\big[M(A_x\phi),(D_x\mu)^2\big]_{ew}+\big[M(A_y\phi),(D_y\mu)^2\big]_{ns}=0, \tag{3.17}$$

where E_h is the discrete energy functional defined as

$$E_h=\frac{1}{2}\|\mathbf{u}\|_2^2+\frac{\gamma\varepsilon}{2}\|\nabla\phi\|_2^2+\frac{\gamma}{\varepsilon}(f(\phi),1)_2. \tag{3.18}$$

Proof. Noticing that $u \in \mathcal{E}_{x \times y}^{ew0}$ and using Lemma 3.1, we have

$$\left[uD_x(a_x u) + A_x(d_x(uu)), u \right]_{ew} = -\left(a_x u, d_x(uu)\right)_2 + \left(d_x(uu), a_x u\right)_2 = 0. \tag{3.19}$$

Eq. (3.7) implies that $u \in \mathcal{E}_{x \times \overline{y}}^{ew0}$, $v \in \mathcal{E}_{\overline{x} \times y}^{ns0}$, and thus $A_x v D_y u, A_y u A_x v \in \mathcal{V}_{x \times y}^0$. According to Lemma 3.2, we then have

$$\left[a_y(A_x v D_y u) + d_y(A_y u A_x v), u \right]_{ew} = \langle A_x v D_y u, A_y u \rangle_{vc} - \langle A_y u A_x v, D_y u \rangle_{vc} = 0. \tag{3.20}$$

Similarly, we can deduce

$$\left[a_x(A_y u D_x v) + d_x(A_y u A_x v), v \right]_{ns} = 0, \quad \left[v D_y(a_y v) + A_y(d_y(vv)), v_2 \right]_{ns} = 0, \tag{3.21}$$

$$[D_x p, u]_{ew} + [D_y p, v]_{ns} = -(p, d_x u + d_y v)_2 = 0, \tag{3.22}$$

$$\left[\eta D_x(d_x u), u \right]_{ew} + \left[\eta D_y(d_y v), v \right]_{ns} = -\left(\eta, (d_x u)^2 + (d_y v)^2 \right)_2, \tag{3.23}$$

$$[A_x \phi D_x \mu, u]_{ew} + [A_y \phi D_y \mu, v]_{ns} = -\left(\mu, d_x(A_x \phi u) + d_y(A_y \phi v) \right)_2, \tag{3.24}$$

$$\left(d_x(M(A_x \phi) D_x \mu) + d_y(M(A_y \phi) D_y \mu), \mu \right)_2 =$$
$$- \left[M(A_x \phi), (D_x \mu)^2 \right]_{ew} - \left[M(A_y \phi), (D_y \mu)^2 \right]_{ns}. \tag{3.25}$$

Computing the discrete inner product of (3.15a), (3.15b) and (3.15d) with u, v and μ, respectively, and using (3.19)-(3.25), we have

$$[u, u_t]_{ew} + [v, v_t]_{ns} + (\mu, \phi_t)_2 =$$
$$- \left(\eta, (d_x u)^2 + (d_y v)^2 \right)_2 - \left[M(A_x \phi), (D_x \mu)^2 \right]_{ew} - \left[M(A_y \phi), (D_y \mu)^2 \right]_{ns}. \tag{3.26}$$

In addition, it is not hard to calculate

$$\frac{d}{dt} E_h = [u, u_t]_{ew} + [v, v_t]_{ns} + \gamma \varepsilon ([D_x \phi, D_x \phi_t]_{ew} + [D_y \phi, D_y \phi_t]_{ns}) + (\frac{\gamma}{\varepsilon} f(\phi), \phi_t)_2$$
$$= [u, u_t]_{ew} + [v, v_t]_{ns} - (\gamma \varepsilon \Delta_h \phi, \phi_t)_2 + (\frac{\gamma}{\varepsilon} f(\phi), \phi_t)_2$$
$$= [u, u_t]_{ew} + [v, v_t]_{ns} + (\mu, \phi_t)_2.$$

Adding the two equations above will lead us to (3.17). This completes the proof. □

4 Decoupled Time Discretization

With the semi-discrete scheme 3.1, we are ready to introduce the temporal discretization. Notice the fact the spatial discretization and temporal discretization are independent. To simply our notations, we apply the temporal discretization directly on the continuous CHNS system (1.3), instead of on the semi-discrete scheme in (3.15a)-(3.15e). However, we emphasize by using the same time discretization on the semi-discrete scheme 3.1, the full discrete scheme will be immediately obtained.

4.1 Notations for temporal discretization

First of all, we introduce some notations for temporal discretization. Consider the time domain $t \in [0,T]$. We discretize it into equally distanced intervals $0 = t_0 < t_1 < t_2 < \cdots < t_N = T$, with $\delta t = \frac{T}{N}$, and $t_i = i \delta t$, $i = 0,1,2 \cdots, N$. Furthermore, we introduce the notations:

$$\phi^{n+\frac{1}{2}} = \frac{1}{2}(\phi^{n+1} + \phi^n), \quad \overline{\phi}^{n+\frac{1}{2}} = \frac{1}{2}(3\phi^n - \phi^{n-1}), \tag{4.1}$$

$$\overline{\phi}^{n+\frac{1}{4}} = \frac{5}{4}\phi^n - \frac{1}{4}\phi^{n-1}, \quad \overline{\phi}^{n+\frac{3}{4}} = \frac{7}{4}\phi^n - \frac{3}{4}\phi^{n-1}, \tag{4.2}$$

$$\tilde{\mathbf{u}}^{n+\frac{1}{2}} = \frac{1}{2}(3\mathbf{u}^n - \mathbf{u}^{n-1}), \quad \overline{\mathbf{u}}^{n+\frac{1}{4}} = \frac{5}{4}\mathbf{u}^n - \frac{1}{4}\mathbf{u}^{n-1}, \quad \overline{\mathbf{u}}^{n+\frac{3}{4}} = \frac{7}{4}\mathbf{u}^n - \frac{3}{4}\mathbf{u}^{n-1}. \tag{4.3}$$

Recall the bulk potential $f(\phi)$ in (1.2). For the semi-implicit discretization of $f'(\phi):=\phi^3-\phi$ in the interval $[t_n,t_{n+1}]$, we denote it as $\frac{\delta f}{\delta(\phi^n,\phi^{n+1})}$. In this paper, we use the classical difference quotient

$$\frac{\delta f}{\delta(\phi^n,\phi^{n+1})}=\Big[\frac{(\phi^n)^2+(\phi^{n+1})^2}{2}-1\Big]\frac{\phi^n+\phi^{n+1}}{2}. \tag{4.4}$$

It has the property that

$$f(\phi^{n+1})-f(\phi^n)=(\phi^{n+1}-\phi^n)\frac{\delta f}{\delta(\phi^n,\phi^{n+1})}. \tag{4.5}$$

The property in (4.5) is a rather strong requirement. In general, we could require a weaker property

$$f(\phi^{n+1})-f(\phi^n)\le(\phi^{n+1}-\phi^n)\frac{\delta f}{\delta(\phi^n,\phi^{n+1})}. \tag{4.6}$$

The advantage of the choice in (4.4) is that the requirement in (4.5) is automatically satisfied. Meanwhile, the major disadvantage is that it is nonlinear, such that each time step, a nonlinear problem has to be solved.

Remark 4.1. The choice of $\frac{\delta f}{\delta(\phi^n,\phi^{n+1})}$ is not unique. If we can assume $\max_{\phi\in\mathbb{R}}|f'(\phi)|\le L$, with L a constant, we can utilize the semi-implicit stabilized discretization to linearize it as

$$\frac{\delta f}{\delta(\phi^n,\phi^{n+1})}=f'(\frac{3}{2}\phi^n-\frac{1}{2}\phi^{n-1})-A\delta t\Delta(\phi^{n+1}-\phi^n)+B(\phi^{n+1}-2\phi^n+\phi^{n-1}), \tag{4.7}$$

where A and B are stabilization constants [39]. It can be shown that the scheme will be energy stable, given A and B is big enough. Or as a simple case, we may use the linearized approximation

$$\frac{\delta f}{\delta(\phi^n,\phi^{n+1})}=f'(\frac{3}{2}\phi^n-\frac{1}{2}\phi^{n-1})+C\delta t(\phi^{n+1}-\phi^n), \tag{4.8}$$

with C a stabilization constant. The possible choices in (4.4), (4.7) and (4.8) all have their advantages and disadvantages. One can even further simplify this by introducing auxiliary variables to result in linear systems [48]. However, the major focus of this paper is to design decoupled numerical schemes such that the CHNS system can be easily solved.

4.2 First-order decoupled schemes

With the reformulation (2.8) in mind, we start with first-order decoupled schemes. Utilizing the classical first-order operator splitting method for the mobility operator $\mathcal{G}$, we have the following result.

Scheme 4.1 (Generic First-order Operator Splitting Scheme). To solve the CHNS system of (2.8) in the time interval $[t_n,t_{n+1}]$, we use the first-order operator splitting method for $\mathcal{G}:=\mathcal{G}_1+\mathcal{G}_2$. Then each time marching step will require the following three sub-steps.

- Step 1: In the interval $[t_n,t_{n+1}]$, solve the problem

$$\Lambda\partial_t\Psi=\mathcal{G}_1\frac{\delta\mathcal{E}}{\delta\Psi}, \text{ with } \Psi(t=t_n)=\Psi^n,$$

    and get $\Psi_\star=\Psi(t=t_{n+1})$.

- Step 2: In the interval $[t_n,t_{n+1}]$, solve the problem

$$\Lambda\partial_t\Psi=\mathcal{G}_2\frac{\delta\mathcal{E}}{\delta\Psi} \text{ with } \Psi(t=t_n)=\Psi_\star,$$

    and get $\Psi^{n+1}=\Psi(t=t_{n+1})$.

Apply (2.10) with $\mathcal{G}_1=\mathcal{G}_a$ and $\mathcal{G}_2=\mathcal{G}_s$ to the first-order scheme 4.1, we get the following specified scheme for the CHNS system.

Scheme 4.2. To solve the CHNS system in $[t_n, t_{n+1}]$, we use the following two steps to obtain $(\mathbf{u}^{n+1}, \phi^{n+1})$ given $(\mathbf{u}^n, \phi^n)$.

- Step 1, in $[t_n, t_{n+1}]$, solve $(\mathbf{u}_*, \phi^{n+1})$ from

$$\frac{\mathbf{u}_* - \mathbf{u}^n}{\delta t} = -\nabla p - \phi^n \nabla \mu^{n+1}, \tag{4.9a}$$

$$\nabla \cdot \mathbf{u}_* = 0, \tag{4.9b}$$

$$\frac{\phi^{n+1} - \phi^n}{\delta t} + \nabla \cdot (\mathbf{u}_* \phi^n) = \nabla \cdot (M(\phi^n) \nabla \mu^{n+1}), \tag{4.9c}$$

$$\mu^{n+1} = \gamma \varepsilon \Delta \phi^{n+1} + \frac{\gamma}{\varepsilon} \frac{\delta f}{\delta(\phi^n, \phi^{n+1})}, \tag{4.9d}$$

$$\mathbf{u}_* = 0, \quad \nabla \phi^{n+1} \cdot \mathbf{n} = 0, \quad \nabla \mu^{n+1} \cdot \mathbf{n} = 0, \text{ on } \partial \Omega. \tag{4.9e}$$

- Step 2, in $[t_n, t_{n+1}]$, solve $\mathbf{u}^{n+1}$ from

$$\frac{\mathbf{u}^{n+1} - \mathbf{u}_*}{\delta t} + B(\mathbf{u}^n, \mathbf{u}^{n+1}) = -\nabla p + \eta \Delta \mathbf{u}^{n+1}, \tag{4.10a}$$

$$\nabla \cdot \mathbf{u}^{n+1} = 0, \tag{4.10b}$$

$$\mathbf{u}_* = 0, \text{ on } \partial \Omega. \tag{4.10c}$$

Theorem 4.1. *The scheme 4.2 is energy stable, in the sense that*

$$\mathcal{E}(\mathbf{u}^{n+1}, \phi^{n+1}) - \mathcal{E}(\mathbf{u}^n m, \phi^n) \leq -\delta t \left[\|\nabla \mathbf{u}^{n+1}\|^2 + \|\sqrt{M(\phi^n)} \nabla \mu^{n+1}\|^2 \right], \tag{4.11}$$

where the energy is defined as

$$\mathcal{E}(\mathbf{u}, \phi) = E(\mathbf{u}) + F(\phi), \quad E(\mathbf{u}) = \int_\Omega \frac{\rho}{2} |\mathbf{u}|^2 d\mathbf{x}, \quad F(\phi) = \gamma \int_\Omega \frac{\varepsilon}{2} |\nabla \phi|^2 + \frac{1}{\varepsilon} f(\phi) d\mathbf{x}.$$

The proof is similar to those in the second-order schemes. Thus we omit the details for brevity. Notice using different splitting techniques for the mobility operator $\mathcal{G}$ will lead to a different class of numerical algorithms.

Remark 4.2. If we reduce the incompressibility constraint in (4.9b), and use velocity projection for (4.10), the resulted scheme will be

- Step 1, in $[t_n, t_{n+1}]$, solve

$$\frac{\mathbf{u}_* - \mathbf{u}^n}{\delta t} = -\phi^n \nabla \mu^{n+1}, \tag{4.12a}$$

$$\frac{\phi_* - \phi^n}{\delta t} + \nabla \cdot (\mathbf{u}_* \phi^n) = \nabla \cdot (M(\phi^n) \nabla \mu^{n+1}), \tag{4.12b}$$

$$\mu^{n+1} = \gamma \varepsilon \Delta \phi^{n+1} + \frac{\gamma}{\varepsilon} \frac{\delta f}{\delta(\phi^n, \phi_*)}, \tag{4.12c}$$

$$\nabla \phi^{n+1} \cdot \mathbf{n} = 0, \quad \nabla \mu^{n+1} \cdot \mathbf{n} = 0, \text{ on } \partial \Omega. \tag{4.12d}$$

- Step 2, in $[t_n, t_{n+1}]$, solve

$$\frac{\mathbf{u}^{n+1} - \mathbf{u}_*}{\delta t} + B(\mathbf{u}^n, \mathbf{u}^{n+1}) = -\nabla p^n + \eta \Delta \mathbf{u}^{n+1}, \tag{4.13a}$$

$$\mathbf{u}_* = 0, \text{ on } \partial \Omega. \tag{4.13b}$$

- Step 3, solve

$$\frac{\mathbf{u}^{n+1} - \mathbf{u}_*}{\delta t} = -(\nabla p^{n+1} - \nabla p^n), \tag{4.14a}$$

$$\nabla \cdot \mathbf{u}^{n+1} = 0, \tag{4.14b}$$

$$\nabla p^{n+1} \cdot \mathbf{n} = 0, \text{ on } \partial \Omega. \tag{4.14c}$$

Notice that Step 1 can be further simplified by eliminating $\mathbf{u}_*$ in (4.12). This reduced scheme is equivalent to the decoupled scheme discussed in [31,38]. In other words, the decoupled schemes in [31,38] can be treated as a special case of first-order operator splitting schemes.

4.3 Second-order decoupled schemes

Next, we focus on developing second-order decoupled schemes for the CHNS system. Specifically, we apply second-order operator splitting techniques to the reformulated model in (2.8).

Scheme 4.3 (Generic Second-order Operator Splitting Scheme). To solve the CHNS system of (2.8) in the time interval $[t_n, t_{n+1}]$, we use the (second-order) Strang-Marchuk operator splitting method for $\mathcal{G} := \mathcal{G}_1 + \mathcal{G}_2$. Then each time marching step will require the following three sub-steps.

- Step 1: In the interval $[t_n, t_{n+\frac{1}{2}}]$, solve the problem

$$\Lambda \partial_t \Psi = \mathcal{G}_1 \frac{\delta \mathcal{E}}{\delta \Psi}, \text{ with } \Psi(t=t_n) = \Psi^n,$$

and get $\Psi_\star = \Psi(t = t_{n+\frac{1}{2}})$.

- Step 2: In the interval $[t_n, t_{n+1}]$, solve the problem

$$\Lambda \partial_t \Psi = \mathcal{G}_2 \frac{\delta \mathcal{E}}{\delta \Psi} \text{ with } \Psi(t=t_n) = \Psi_\star,$$

and get $\Psi_{\star\star} = \Psi(t = t_{n+1})$.

- Step 3: In the interval $[t_{n+\frac{1}{2}}, t_{n+1}]$, solve the problem

$$\Lambda \partial_t \Psi = \mathcal{G}_1 \frac{\delta \mathcal{E}}{\delta \Psi}, \text{ with } \Psi(t=t_{n+\frac{1}{2}}) = \Psi_{\star\star}.$$

and get $\Psi^{n+1} = \Psi(t_{n+1})$.

The scheme above is a second-order operator splitting algorithm. Given specific operators $\mathcal{G} := \mathcal{G}_1 + \mathcal{G}_2$, the proposed scheme 4.3 can be specified. In the rest of this section, we will discuss several variants of decoupled numerical schemes.

4.3.1 Second-order decoupled time-marching scheme for the CHNS model

If we plug the mobility operator splitting formula (2.9) into the general scheme 4.3, we obtain the second-order numerical schemes below.

Scheme 4.4. Given $(\mathbf{u}^n, \phi^n)$, $(\mathbf{u}^{n-1}, \phi^{n-1})$ and $\mathbf{u}^n \cdot \mathbf{n} = 0$, we can obtain $(\mathbf{u}^{n+1}, \phi^{n+1})$ in the following three steps:

- Step 1: in $[t_n, t_{n+\frac{1}{2}}]$, we solve $(\mathbf{u}_\star, \phi_\star)$ via the following two decoupled sub-steps.

  - Step 1.1: solve $\mathbf{u}_\star$ via

$$\rho \frac{\mathbf{u}_\star - \mathbf{u}^n}{\delta t/2} + B(\bar{\mathbf{u}}^{n+\frac{1}{4}}, \frac{\mathbf{u}_\star + \mathbf{u}^n}{2}) = -\nabla p + \eta \Delta \frac{\mathbf{u}_\star + \mathbf{u}^n}{2}, \tag{4.15a}$$

$$\nabla \cdot \frac{\mathbf{u}_\star + \mathbf{u}^n}{2} = 0, \tag{4.15b}$$

$$\mathbf{u}_\star = 0, \quad \text{on } \partial\Omega. \tag{4.15c}$$

  - Step 1.2: solve $\phi_\star$ via

$$\frac{\phi_\star - \phi^n}{\delta t/2} = \nabla(M(\bar{\phi}^{n+\frac{1}{4}}) \nabla \mu^{n+\frac{1}{4}}), \tag{4.16a}$$

$$\mu^{n+\frac{1}{4}} = -\frac{\gamma \varepsilon}{2}(\Delta \phi_\star + \Delta \phi^n) + \frac{\gamma}{\varepsilon} \frac{\delta f}{\delta(\phi^n, \phi_\star)}, \tag{4.16b}$$

$$\nabla \mu^{n+\frac{1}{4}} \cdot \mathbf{n} = 0, \quad \nabla \phi_\star \cdot \mathbf{n} = 0, \quad \text{on } \partial\Omega. \tag{4.16c}$$

- Step 2, In $[t_n, t_{n+1}]$, we solve $(\mathbf{u}_{\star\star}, \phi_{\star\star})$ via two sub-steps.

  – Step 2.1, Solve $(\phi_{\star\star}, p)$ via the following system

$$\frac{1}{\delta t}(\phi_{\star\star} - \phi_\star) + \nabla \cdot (\mathbf{u}_\star \overline{\phi}^{n+\frac{1}{2}}) = \nabla \cdot (\frac{\delta t}{2\rho}(\overline{\phi}^{n+\frac{1}{2}})^2 \nabla \mu^{n+\frac{1}{2}}) + \frac{\delta t}{2\rho} \nabla \cdot (\overline{\phi}^{n+\frac{1}{2}} \nabla p), \qquad (4.17a)$$

$$\mu^{n+\frac{1}{2}} = -\frac{\gamma\varepsilon}{2}(\Delta\phi_{\star\star} + \Delta\phi_\star) + \frac{\gamma}{\varepsilon}\frac{\delta f}{\delta(\phi_\star, \phi_{\star\star})}, \qquad (4.17b)$$

$$-\Delta p - \nabla \cdot (\overline{\phi}^{n+\frac{1}{2}} \nabla \mu^{n+\frac{1}{2}}) = 0, \qquad (4.17c)$$

$$\nabla\mu^{n+\frac{1}{2}} \cdot \mathbf{n} = 0, \quad \nabla\phi_{\star\star} \cdot \mathbf{n} = 0, \quad \nabla p \cdot \mathbf{n} = 0, \quad \text{on } \partial\Omega. \qquad (4.17d)$$

  – Step 2.2, Update $\mathbf{u}_{\star\star}$ via

$$\mathbf{u}_{\star\star} = \mathbf{u}_\star - \frac{\delta t}{\rho}(\nabla p + \overline{\phi}^{n+\frac{1}{2}} \nabla\mu^{n+\frac{1}{2}}), \qquad (4.18)$$

  with $\mu^{n+\frac{1}{2}}$ defined in (4.17).

- Step 3, In $[t_{n+\frac{1}{2}}, t_{n+1}]$, we solve $(\mathbf{u}^{n+1}, \phi^{n+1})$ via the following decoupled two sub-steps.

  – Step 3.1, Solve $\mathbf{u}^{n+1}$ via

$$\rho\frac{\mathbf{u}^{n+1} - \mathbf{u}_{\star\star}}{\delta t/2} + B(\overline{\mathbf{u}}^{n+\frac{3}{4}}, \frac{\mathbf{u}^{n+1} + \mathbf{u}_{\star\star}}{2}) = -\nabla p + \eta\Delta\frac{\mathbf{u}_{\star\star} + \mathbf{u}^{n+1}}{2}, \qquad (4.19a)$$

$$\nabla \cdot \frac{\mathbf{u}^{n+1} + \mathbf{u}_{\star\star}}{2} = 0, \qquad (4.19b)$$

$$\mathbf{u}^{n+1} = 0, \quad \text{on } \partial\Omega. \qquad (4.19c)$$

  – Step 3.2, Solve ϕ^{n+1} via

$$\frac{\phi^{n+1} - \phi_{\star\star}}{\delta t/2} = \nabla \cdot (M(\overline{\phi}^{n+\frac{3}{4}})\nabla\mu^{n+\frac{3}{4}}), \qquad (4.20a)$$

$$\mu^{n+\frac{3}{4}} = -\frac{\gamma\varepsilon}{2}(\Delta\phi^{n+1} + \Delta\phi_{\star\star}) + \frac{\gamma}{\varepsilon}\frac{\delta f}{\delta(\phi_{\star\star}, \phi^{n+1})}, \qquad (4.20b)$$

$$\nabla\mu^{n+\frac{3}{4}} \cdot \mathbf{n} = 0, \quad \nabla\phi^{n+1} \cdot \mathbf{n} = 0, \quad \text{on } \partial\Omega. \qquad (4.20c)$$

The scheme above is second-order accurate in time. Moreover, in each step, only problems with smaller sizes need to be solved. Here are several remarks.

Remark 4.3. Step 2 in (4.17)-(4.18) comes from the problem

$$\rho\frac{\mathbf{u}_{\star\star} - \mathbf{u}_\star}{\delta t} = -\nabla p - \overline{\phi}^{n+\frac{1}{2}}\nabla\mu^{n+\frac{1}{2}}, \qquad (4.21a)$$

$$\mu^{n+\frac{1}{2}} = -\frac{\gamma\varepsilon}{2}(\Delta\phi_{\star\star} + \Delta\phi_\star) + \frac{\gamma}{\varepsilon}\frac{\delta f}{\delta(\phi_\star, \phi_{\star\star})}, \qquad (4.21b)$$

$$\nabla \cdot \frac{\mathbf{u}_{\star\star} + \mathbf{u}_\star}{2} = 0, \qquad (4.21c)$$

$$\frac{\phi_{\star\star} - \phi_\star}{\delta t} = -\nabla \cdot (\frac{\mathbf{u}_{\star\star} + \mathbf{u}_\star}{2}\overline{\phi}^{n+\frac{1}{2}}), \qquad (4.21d)$$

$$\nabla\mu^{n+\frac{1}{2}} \cdot \mathbf{n} = 0, \quad \nabla\phi_{\star\star} \cdot \mathbf{n} = 0, \quad \mathbf{u}_{\star\star} = 0, \quad \text{on } \partial\Omega. \qquad (4.21e)$$

Notice $\mathbf{u}_{\star\star}$ and $\phi_{\star\star}$ can be decoupled, by realizing the following equality

$$\frac{\mathbf{u}_{\star\star} + \mathbf{u}_\star}{2} = \mathbf{u}_\star - \frac{\delta t}{2\rho}(\nabla p + \overline{\phi}^{n+\frac{1}{2}}\nabla\mu^{n+\frac{1}{2}}).$$

Then we rewrite the problem in Step 2 as two decoupled sub-steps in (4.17)-(4.18). The coupled system of $(\phi_{\star\star}, p)$ is significantly reduced compared with the original coupled CHNS system in (1.3).

Remark 4.4. Furthermore, we can even relax the in-compressibility constraint in Step 2. Then the problem of (4.21) in Step 2 is reduced to

$$
\begin{cases}
\rho \frac{\mathbf{u}_{\star\star} - \mathbf{u}_\star}{\delta t} = -\bar{\phi}^{n+\frac{1}{2}} \nabla \mu^{n+\frac{1}{2}}, \\
\mu^{n+\frac{1}{2}} = -\frac{\gamma\varepsilon}{2}(\Delta\phi_{\star\star} + \Delta\phi_\star) + \frac{\gamma}{\varepsilon}\frac{\delta f}{\delta(\phi_\star,\phi_{\star\star})}, \\
\frac{\phi_{\star\star} - \phi_\star}{\delta t} = -\nabla \cdot \left(\frac{\mathbf{u}_{\star\star} + \mathbf{u}_\star}{2}\bar{\phi}^{n+\frac{1}{2}}\right), \\
\nabla \mu^{n+\frac{1}{2}} \cdot \mathbf{n} = 0, \quad \nabla\phi_{\star\star} \cdot \mathbf{n} = 0, \quad \mathbf{u}_{\star\star} = 0, \quad \text{on } \partial\Omega.
\end{cases}
\tag{4.22}
$$

Hence, Step 2 can be solved by the following two sub-steps:

- Step 2.1, solve $\phi_{\star\star}$ via

$$
\begin{cases}
\frac{1}{\delta t}(\phi_{\star\star} - \phi_\star) + \nabla \cdot (\mathbf{u}_\star \bar{\phi}^{n+\frac{1}{2}}) = \nabla \cdot \left(\frac{\delta t}{2\rho}(\bar{\phi}^{n+\frac{1}{2}})^2 \nabla\mu^{n+\frac{1}{2}}\right), \\
\mu^{n+\frac{1}{2}} = -\frac{\gamma\varepsilon}{2}(\Delta\phi_{\star\star} + \Delta\phi_\star) + \frac{\gamma}{\varepsilon}\frac{\delta f}{\delta(\phi_\star,\phi_{\star\star})}, \\
\nabla\mu^{n+\frac{1}{2}} \cdot \mathbf{n} = 0, \quad \nabla\phi_{\star\star} \cdot \mathbf{n} = 0, \quad \text{on } \partial\Omega.
\end{cases}
\tag{4.23}
$$

- Step 2.2, update $\mathbf{u}_{\star\star}$ via

$$
\mathbf{u}_{\star\star} = \mathbf{u}_\star - \frac{\delta t}{\rho}\bar{\phi}^{n+\frac{1}{2}}\nabla\mu^{n+\frac{1}{2}}.
\tag{4.24}
$$

Since scheme 4.4 is already easy to solve, we don't attempt this relaxation strategy in this paper. Interested readers are encouraged to explore it further.

Theorem 4.1 (Energy Stability). *The proposed scheme 4.4 is energy stable, in the sense that*

$$
\mathcal{E}(\mathbf{u}^{n+1},\phi^{n+1}) - \mathcal{E}(\mathbf{u}^n,\phi^n) \leq -\frac{\delta t}{2}\left[\eta\|\nabla\frac{\mathbf{u}_\star + \mathbf{u}^n}{2}\|^2 + \eta\|\nabla\frac{\mathbf{u}^{n+1} + \mathbf{u}_{\star\star}}{2}\|^2\right.
$$
$$
\left. + \|\sqrt{M(\bar{\phi}^{n+\frac{1}{4}})}\nabla\mu^{n+\frac{1}{4}}\|^2 + \|\sqrt{M(\bar{\phi}^{n+\frac{3}{4}})}\nabla\mu^{n+\frac{3}{4}}\|^2\right], \tag{4.25}
$$

where the energy is defined as

$$
\mathcal{E}(\mathbf{u},\phi) = E(\mathbf{u}) + F(\phi), \quad E(\mathbf{u}) = \int_\Omega \frac{\rho}{2}|\mathbf{u}|^2 d\mathbf{x}, \quad F(\phi) = \gamma\int_\Omega \frac{\varepsilon}{2}|\nabla\phi|^2 + \frac{1}{\varepsilon}f(\phi)d\mathbf{x}.
\tag{4.26}
$$

Proof. If we take inner product of (4.15a) with $\frac{\delta t}{2}\frac{\mathbf{u}_\star + \mathbf{u}^n}{2}$ and apply the boundary conditions in (4.15c), we will have

$$
E(\mathbf{u}_\star) - E(\mathbf{u}^n) = -\frac{\delta t}{2}\left(\frac{\mathbf{u}_\star + \mathbf{u}^n}{2}, \nabla p\right) - \frac{\delta t}{2}\eta\|\nabla\frac{\mathbf{u}_\star + \mathbf{u}^n}{2}\|^2.
\tag{4.27}
$$

If we take inner product of (4.15b) with $\frac{\delta t}{2}p$, we have

$$
\frac{\delta t}{2}\left(p, \nabla \cdot \frac{\mathbf{u}_\star + \mathbf{u}^n}{2}\right) = 0.
\tag{4.28}
$$

Then, adding the two equations in (4.27) and (4.28) above, we get

$$
E(\mathbf{u}_\star) - E(\mathbf{u}^n) = -\frac{\delta t}{2}\eta\|\nabla\frac{\mathbf{u}_\star + \mathbf{u}^n}{2}\|^2,
\tag{4.29}
$$

by noticing the boundary condition (4.15c) and $\mathbf{u}^n \cdot \mathbf{n} = 0$.

Similarly, if we take inner product of (4.16a) with $\frac{\delta t}{2}\mu^{n+\frac{1}{4}}$, and inner product of (4.16b) with $\phi_\star - \phi^n$, apply the boundary condition in (4.16c), and use the constraint (4.5), we have

$$
F(\phi_\star) - F(\phi^n) = -\frac{\delta t}{2}\|\sqrt{M(\bar{\phi}^{n+\frac{1}{4}})}\nabla\mu^{n+\frac{1}{4}}\|^2.
\tag{4.30}
$$

The two equations above give us

$$\mathcal{E}(\mathbf{u}_\star, \phi_\star) - \mathcal{E}(\mathbf{u}^n, \phi^n) = -\frac{\delta t}{2}\left[\eta\|\nabla\frac{\mathbf{u}_\star + \mathbf{u}^n}{2}\|^2 + \|\sqrt{M(\overline{\phi}^{n+\frac{1}{4}})}\nabla\mu^{n+\frac{1}{4}}\|^2\right]. \tag{4.31}$$

Given that (4.17)-(4.18) is equivalent to (4.21). We take inner product of (4.21a) with $\delta t\frac{\mathbf{u}_{\star\star}+\mathbf{u}_\star}{2}$, inner product of (4.21b) with $(\phi_{\star\star} - \phi_\star)$, inner product of (4.21c) with p and inner product of (4.21d) with $\delta t\mu^{n+\frac{1}{2}}$, and utilize the boundary conditions in (4.21e), we will get

$$\mathcal{E}(\mathbf{u}_{\star\star}, \phi_{\star\star}) - \mathcal{E}(\mathbf{u}_\star, \phi_\star) = 0. \tag{4.32}$$

In a similar manner, we take inner product of (4.19a) with $\frac{\delta t}{2}\frac{\mathbf{u}^{n+1}+\mathbf{u}_{\star\star}}{2}$, (4.19b) with p, we will get

$$E(\mathbf{u}^{n+1}) - E(\mathbf{u}_{\star\star}) = -\frac{\delta t}{2}\eta\|\nabla\frac{\mathbf{u}^{n+1}+\mathbf{u}_{\star\star}}{2}\|^2. \tag{4.33}$$

And if we take inner product of (4.20a) with $\frac{\delta t}{2}\mu^{n+\frac{3}{4}}$ and (4.20b) with $\phi^{n+1} - \phi_{\star\star}$, we will obtain

$$F(\phi^{n+1}) - F(\phi_{\star\star}) = -\frac{\delta t}{2}\|\sqrt{M(\overline{\phi}^{n+\frac{3}{4}})}\nabla\mu^{n+\frac{3}{4}}\|^2. \tag{4.34}$$

Adding (4.33) and (4.34), we have

$$\mathcal{E}(\mathbf{u}^{n+1}, \phi^{n+1}) - \mathcal{E}(\mathbf{u}_{\star\star}, \phi_{\star\star}) = -\frac{\delta t}{2}\left[\eta\|\nabla\frac{\mathbf{u}^{n+1}+\mathbf{u}_{\star\star}}{2}\|^2 + \|\sqrt{M(\overline{\phi}^{n+\frac{3}{4}})}\nabla\mu^{n+\frac{3}{4}}\|^2\right]. \tag{4.35}$$

Overall, if we add the three equations in (4.31), (4.32) and (4.35) together, the discrete energy law is obtained as

$$\mathcal{E}(\mathbf{u}^{n+1}, \phi^{n+1}) - \mathcal{E}(\mathbf{u}^n, \phi^n) \leq -\frac{\delta t}{2}\Big[\eta\|\nabla\frac{\mathbf{u}_\star + \mathbf{u}^n}{2}\|^2 + \eta\|\nabla\frac{\mathbf{u}^{n+1}+\mathbf{u}_{\star\star}}{2}\|^2$$
$$+ \|\sqrt{M(\overline{\phi}^{n+\frac{1}{4}})}\nabla\mu^{n+\frac{1}{4}}\|^2 + \|\sqrt{M(\overline{\phi}^{n+\frac{3}{4}})}\nabla\mu^{n+\frac{3}{4}}\|^2\Big]. \tag{4.36}$$

$\square$

4.3.2 An alternative second-order decoupled numerical scheme based on a different operator splitting strategy

In the meanwhile, if we plug in the splitting operators defined in (2.10), we obtain the following second-order operator splitting scheme.

Scheme 4.5. Given $(\mathbf{u}^n, \phi^n)$, $(\mathbf{u}^{n-1}, \phi^{n-1})$ and $\mathbf{u}^n \cdot \mathbf{n} = 0$, we can obtain $(\mathbf{u}^{n+1}, \phi^{n+1})$ in the following three steps:

• Step 1: In $[t_n, t_{n+\frac{1}{2}}]$, we set $\phi_\star = \phi^n$, and solve $\mathbf{u}_\star$ via

$$\rho\frac{\mathbf{u}_\star - \mathbf{u}^n}{\delta t/2} + B(\bar{\mathbf{u}}^{n+\frac{1}{4}}, \frac{\mathbf{u}_\star + \mathbf{u}^n}{2}) = -\nabla p + \eta\Delta\frac{\mathbf{u}_\star + \mathbf{u}^n}{2}, \tag{4.37a}$$

$$\nabla\cdot\frac{\mathbf{u}_\star + \mathbf{u}^n}{2} = 0, \tag{4.37b}$$

$$\mathbf{u}_\star = 0, \quad \text{on } \partial\Omega. \tag{4.37c}$$

• Step 2, In $[t_n, t_{n+1}]$, we solve $(\mathbf{u}_{\star\star}, \phi_{\star\star})$ via the following two sub-steps.

– Step 2.1, Solve $(\phi_{\star\star}, p)$ via the following system

$$\frac{1}{\delta t}(\phi_{\star\star} - \phi_\star) + \nabla\cdot(\mathbf{u}_\star\overline{\phi}^{n+\frac{1}{2}}) = \tag{4.38a}$$
$$\nabla\cdot((M(\overline{\phi}^{n+\frac{1}{2}}) + \frac{\delta t}{2\rho}(\overline{\phi}^{n+\frac{1}{2}})^2)\nabla\mu^{n+\frac{1}{2}}) + \frac{\delta t}{2\rho}\nabla\cdot(\overline{\phi}^{n+\frac{1}{2}}\nabla p),$$

$$\mu^{n+\frac{1}{2}} = -\frac{\gamma\varepsilon}{2}(\Delta\phi_{\star\star} + \Delta\phi_\star) + \frac{\gamma}{\varepsilon}\frac{\delta f}{\delta(\phi_\star, \phi_{\star\star})}, \tag{4.38b}$$

$$-\Delta p - \nabla\cdot(\overline{\phi}^{n+\frac{1}{2}}\nabla\mu^{n+\frac{1}{2}}) = 0, \tag{4.38c}$$

$$\nabla\mu^{n+\frac{1}{2}}\cdot\mathbf{n} = 0, \quad \nabla\phi^{n+1}\cdot\mathbf{n} = 0, \quad \nabla p\cdot\mathbf{n} = 0, \quad \text{on } \partial\Omega. \tag{4.38d}$$

– Step 2.2, Update $\mathbf{u}_{\star\star}$ via

$$\mathbf{u}_{\star\star}=\mathbf{u}_{\star}-\frac{\delta t}{\rho}(\nabla p+\bar{\phi}^{n+\frac{1}{2}}\nabla\mu^{n+\frac{1}{2}}). \tag{4.39}$$

- Step 3, In $[t_{n+\frac{1}{2}},t_{n+1}]$, we set $\phi^{n+1}=\phi_{\star\star}$, and solve $\mathbf{u}^{n+1}$ via

$$\rho\frac{\mathbf{u}^{n+1}-\mathbf{u}_{\star\star}}{\delta t/2}+B(\bar{\mathbf{u}}^{n+\frac{3}{4}},\frac{\mathbf{u}^{n+1}+\mathbf{u}_{\star\star}}{2})=-\nabla p+\eta\Delta\frac{\mathbf{u}_{\star\star}+\mathbf{u}^{n+1}}{2}, \tag{4.40a}$$

$$\nabla\cdot\mathbf{u}^{n+1}=0, \tag{4.40b}$$

$$\mathbf{u}^{n+1}=0, \quad \text{on } \partial\Omega. \tag{4.40c}$$

The scheme 4.5 is computationally efficient than the scheme 4.4 since the phase-field equation only needs to be solved once. In the scheme 4.4, the phase-field equations have to be solved three times.

Remark 4.5. Notice that (4.38)-(4.39) is derived from the problem

$$\rho\frac{\mathbf{u}_{\star\star}-\mathbf{u}_{\star}}{\delta t}=-\nabla p-\bar{\phi}^{n+\frac{1}{2}}\nabla\mu^{n+\frac{1}{2}}, \tag{4.41a}$$

$$\nabla\cdot\mathbf{u}_{\star\star}=0, \tag{4.41b}$$

$$\frac{\phi_{\star\star}-\phi_{\star}}{\delta t}=-\nabla\cdot(\frac{\mathbf{u}_{\star\star}+\mathbf{u}_{\star}}{2}\bar{\phi}^{n+\frac{1}{2}})+\nabla\cdot(M(\bar{\phi}^{n+\frac{1}{2}})\nabla\mu^{n+\frac{1}{2}}), \tag{4.41c}$$

$$\mu^{n+\frac{1}{2}}=-\frac{\gamma\varepsilon}{2}(\Delta\phi_{\star\star}+\Delta\phi_{\star})+\frac{\gamma}{\varepsilon}\frac{\delta f}{\delta(\phi_{\star},\phi_{\star\star})}, \tag{4.41d}$$

$$\nabla\mu^{n+\frac{1}{2}}\cdot\mathbf{n}=0, \quad \nabla\phi_{\star\star}\cdot\mathbf{n}=0, \quad \mathbf{u}_{\star\star}=0, \quad \text{on } \partial\Omega. \tag{4.41e}$$

Remark 4.6. Similarly, as discussed in Remark 4.4, we can introduce relaxation in Step 2. As a minor modification, we do not necessarily need to restrict the in-compressibility during the operator splitting. With that in mind, we can obtain a relaxed version of Step 2 such that a simplified numerical scheme can be proposed. This idea will not be further elaborated due to space limitations.

Theorem 4.2. *The proposed scheme 4.5 is energy stable, in the sense that*

$$\mathcal{E}(\mathbf{u}^{n+1},\phi^{n+1})-\mathcal{E}(\mathbf{u}^n,\phi^n)\leq$$
$$-\frac{\delta t}{2}\Big[\eta\|\nabla\frac{\mathbf{u}_{\star}+\mathbf{u}^n}{2}\|^2+\eta\|\nabla\frac{\mathbf{u}^{n+1}+\mathbf{u}_{\star\star}}{2}\|^2+2\|\sqrt{M(\bar{\phi}^{n+\frac{1}{2}})}\nabla\mu^{n+\frac{1}{2}}\|^2\Big], \tag{4.42}$$

where the energy is defined as

$$\mathcal{E}(\mathbf{u},\phi)=E(\mathbf{u})+F(\phi), \quad E(\mathbf{u})=\int_{\Omega}\frac{\rho}{2}|\mathbf{u}|^2d\mathbf{x}, \quad F(\phi)=\gamma\int_{\Omega}\frac{\varepsilon}{2}|\nabla\phi|^2+\frac{1}{\varepsilon}f(\phi)d\mathbf{x}. \tag{4.43}$$

Hence the scheme is energy stable with the total energy $\mathcal{E}(\mathbf{u}^{n+1},\phi^{n+1})$ non-increasing in time.

Proof. The proof is similar to the proof in Theorem 4.1. Here we only show the major steps. If we take inner product of (4.37a) with $\frac{\delta t}{2}\frac{\mathbf{u}_{\star}+\mathbf{u}^n}{2}$, we will have

$$E(\mathbf{u}_{\star})-E(\mathbf{u}^n)=-\frac{\delta t}{2}(\nabla p,\frac{\mathbf{u}_{\star}+\mathbf{u}^n}{2})-\frac{\delta t}{2}\eta\|\nabla\frac{\mathbf{u}_{\star}+\mathbf{u}^n}{2}\|^2. \tag{4.44}$$

If we take the inner product of (4.37b) with $\frac{\delta t}{2}p$, we have

$$\frac{\delta t}{2}(p,\nabla\cdot\frac{\mathbf{u}_{\star}+\mathbf{u}^n}{2})=0. \tag{4.45}$$

Adding the equations (4.44) and (4.45) above, we get

$$E(\mathbf{u}_{\star})-E(\mathbf{u}^n)=-\frac{\delta t}{2}\eta\|\nabla\frac{\mathbf{u}_{\star}+\mathbf{u}^n}{2}\|^2. \tag{4.46}$$

Given the notations $\phi_\star = \phi^n$, (4.46) is equivalent to

$$\mathcal{E}(\mathbf{u}_\star, \phi_\star) - \mathcal{E}(\mathbf{u}^n, \phi^n) = -\frac{\delta t}{2} \eta \| \nabla \frac{\mathbf{u}_\star + \mathbf{u}^n}{2} \|^2. \tag{4.47}$$

Similarly, if we take inner product of (4.41a) with $\delta t \frac{\mathbf{u}_{\star\star} + \mathbf{u}_\star}{2}$, we will have

$$E(\mathbf{u}_{\star\star}) - E(\mathbf{u}_\star) = -\frac{\delta t}{2}\left(\frac{\mathbf{u}_{\star\star} + \mathbf{u}_\star}{2}, \nabla p\right) - \delta t \left(\frac{\mathbf{u}_{\star\star} + \mathbf{u}_\star}{2}, \overline{\phi}^{n+\frac{1}{2}} \nabla \mu^{n+\frac{1}{2}}\right). \tag{4.48}$$

If we take inner product of (4.41b) with $\frac{\delta t}{2} p$, we have

$$\frac{\delta t}{2}\left(p, \nabla \cdot \frac{\mathbf{u}_{\star\star} + \mathbf{u}_\star}{2}\right) = 0. \tag{4.49}$$

If we take inner product of (4.41c) with $\delta t \mu^{n+\frac{1}{2}}$, and (4.41d) with $\delta t(\phi_{\star\star} - \phi_\star)$, we have

$$F(\phi_{\star\star}) - F(\phi_\star) = -\delta t \left(\nabla \cdot \left(\frac{\mathbf{u}_{\star\star} + \mathbf{u}_\star}{2}\overline{\phi}^{n+\frac{1}{2}}\right), \mu^{n+\frac{1}{2}}\right) - \delta t \| \sqrt{M(\overline{\phi}^{n+\frac{1}{2}})} \nabla \mu^{n+\frac{1}{2}} \|^2. \tag{4.50}$$

Adding the equations (4.48), (4.49) and (4.50) above, we have

$$\mathcal{E}(\mathbf{u}_{\star\star}, \phi_{\star\star}) - \mathcal{E}(\mathbf{u}_\star, \phi_\star) = -\delta t \| \sqrt{M(\overline{\phi}^{n+\frac{1}{2}})} \nabla \mu^{n+\frac{1}{2}} \|^2. \tag{4.51}$$

Similarly, for Step 3, if we take inner product of (4.40a) with $\frac{\delta t}{2} \frac{\mathbf{u}^{n+1} + \mathbf{u}_{\star\star}}{2}$, and take inner product of (4.40b) with δp, we have

$$\mathcal{E}(\mathbf{u}^{n+1}, \phi^{n+1}) - \mathcal{E}(\mathbf{u}_{\star\star}, \phi_{\star\star}) = -\frac{\delta t}{2} \eta \| \nabla \frac{\mathbf{u}^{n+1} + \mathbf{u}_{\star\star}}{2} \|^2. \tag{4.52}$$

Adding the equations (4.47), (4.51) and (4.52) together, we finally obtain the energy dissipation law

$$\mathcal{E}(\mathbf{u}^{n+1}, \phi^{n+1}) - \mathcal{E}(\mathbf{u}^n, \phi^n) \leq$$
$$-\frac{\delta t}{2}\left[\eta \| \nabla \frac{\mathbf{u}_\star + \mathbf{u}^n}{2} \|^2 + \eta \| \nabla \frac{\mathbf{u}^{n+1} + \mathbf{u}_{\star\star}}{2} \|^2 + 2\| \sqrt{M(\overline{\phi}^{n+\frac{1}{2}})} \nabla \mu^{n+\frac{1}{2}} \|^2\right]. \tag{4.53}$$

$\square$

4.4 Strategies to solve the Navier-Stokes equation

In the previous sub-sections, we introduce schemes that decouple the velocity fields and the phase variables. This sub-section further discusses how the Navier-Stoke portion in Step 1 and Step 3 of the proposed schemes can be solved effectively. Recall the Crank-Nicolson (CN) type scheme for the Navier-Stokes equation

$$\begin{cases} \rho \frac{\mathbf{u}^{n+1} - \mathbf{u}^n}{\delta t} + \rho B(\overline{\mathbf{u}}^{n+\frac{1}{2}}, \mathbf{u}^{n+\frac{1}{2}}) = -\nabla p^{n+\frac{1}{2}} + \eta \Delta \mathbf{u}^{n+\frac{1}{2}} + f^{n+\frac{1}{2}}, \\ \nabla \cdot \mathbf{u}^{n+\frac{1}{2}} = 0. \end{cases} \tag{4.54}$$

Here f is the external force term. This paper introduces two strategies: (1) the preconditioner method; (2) the velocity projection method.

4.4.1 Projection method as a preconditioner for the Naver-Stokes equation

First of all, we discuss the precondition strategy. Notice $p^{n+\frac{1}{2}}$ is a Lagrangian multiplier, so it is not advisable to do time marching for p, saying $p^{n+\frac{1}{2}} = \frac{1}{2}(p^n + p^{n+1})$. Instead, we treat $p^{n+\frac{1}{2}}$ as a variable and solve it directly. Therefore, the Navier-Stokes portion in (4.54) can be written as

$$\begin{bmatrix} \frac{2\rho}{\delta t} - \eta\Delta + \rho B^{n+1} & \nabla \\ \nabla \cdot & 0 \end{bmatrix} \begin{pmatrix} \mathbf{u}^{n+\frac{1}{2}} \\ p^{n+\frac{1}{2}} \end{pmatrix} = \begin{bmatrix} \frac{2\rho}{\delta t} + \rho B^n & 0 \\ 0 & 0 \end{bmatrix} \begin{pmatrix} \mathbf{u}^n \\ 0 \end{pmatrix} + \begin{bmatrix} f^{n+\frac{1}{2}} \\ 0 \end{bmatrix}. \tag{4.55}$$

Here B^{n+1} and B^n are generic notations to represent the implicit and explicit parts in the convection operator $B(\overline{\mathbf{u}}^{n+\frac{1}{2}}, \mathbf{u}^{n+\frac{1}{2}})$. To solve the system above, one need an efficient preconditioner. In this paper, we utilize the idea in [16] for solving scheme 4.4 and scheme 4.5. Here we briefly explain how the preconditioner can be constructed.

Recall the decoupled projection scheme for the Navier-Stokes equation in two steps:

- Step 1, solve the intermediate velocity field via

$$2\rho \frac{\tilde{\mathbf{u}}^{n+\frac{1}{2}} - \mathbf{u}^n}{\delta t} + \rho B(\overline{\mathbf{u}}^{n+\frac{1}{2}}, \tilde{\mathbf{u}}^{n+\frac{1}{2}}) = \eta \Delta \tilde{\mathbf{u}}^{n+\frac{1}{2}} + f^{n+\frac{1}{2}}, \tag{4.56}$$

where $\tilde{\mathbf{u}}^{n+\frac{1}{2}} = \frac{1}{2}(\tilde{\mathbf{u}}^{n+1} + \mathbf{u}^n)$.

- Step 2, solve the velocity field via the projection

$$2\rho \frac{\mathbf{u}^{n+\frac{1}{2}} - \tilde{\mathbf{u}}^{n+\frac{1}{2}}}{\delta t} = -\nabla \psi,$$
$$\nabla \cdot \mathbf{u}^{n+1} = 0. \tag{4.57}$$

We can further rewrite (4.56) as

$$\begin{bmatrix} \frac{2\rho}{\delta t} - \eta\Delta + \rho B^{n+1} & 0 \\ 0 & \mathbf{I} \end{bmatrix} \begin{pmatrix} \tilde{\mathbf{u}}^{n+\frac{1}{2}} \\ 0 \end{pmatrix} = \begin{bmatrix} \frac{2\rho}{\delta t} + \rho B^n & 0 \\ 0 & 0 \end{bmatrix} \begin{pmatrix} \mathbf{u}^n \\ 0 \end{pmatrix} + \begin{bmatrix} f^{n+\frac{1}{2}} \\ 0 \end{bmatrix}, \tag{4.58}$$

For (4.57), it can be decomposed into

$$-\Delta\psi = -\frac{2\rho}{\delta t}\nabla \cdot \tilde{\mathbf{u}}^{n+\frac{1}{2}}, \tag{4.59a}$$

$$\mathbf{u}^{n+\frac{1}{2}} = \tilde{\mathbf{u}}^{n+\frac{1}{2}} - \frac{\delta t}{2\rho}\nabla\psi, \tag{4.59b}$$

$$\nabla p^{n+\frac{1}{2}} = \nabla\psi - \frac{\delta t}{\rho}\frac{\eta}{2}\Delta\nabla\psi. \tag{4.59c}$$

Then the corresponding operator forms are given as

$$\begin{bmatrix} \mathbf{I} & 0 \\ 0 & -\Delta \end{bmatrix} \begin{pmatrix} \tilde{\mathbf{u}}^{n+\frac{1}{2}} \\ \psi \end{pmatrix} = \begin{bmatrix} \mathbf{I} & 0 \\ -\frac{2\rho}{\delta t}\nabla \cdot & -\frac{\rho}{\delta t} \end{bmatrix} \begin{pmatrix} \tilde{\mathbf{u}}^{n+\frac{1}{2}} \\ 0 \end{pmatrix}, \tag{4.60a}$$

$$\begin{pmatrix} \mathbf{u}^{n+1} \\ p^{n+\frac{1}{2}} \end{pmatrix} = \begin{bmatrix} \mathbf{I} & -\frac{\delta t}{2\rho}\nabla \\ 0 & \mathbf{I} - \frac{\delta t}{\rho}\frac{\eta}{2}\Delta \end{bmatrix} \begin{pmatrix} \tilde{\mathbf{u}}^{n+1} \\ \psi \end{pmatrix}. \tag{4.60b}$$

Therefore, the two-step procedure (4.56)-(4.57) can be written in an operator form as

$$\mathcal{A}\begin{pmatrix} \mathbf{u}^{n+\frac{1}{2}} \\ p^{n+\frac{1}{2}} \end{pmatrix} = \begin{bmatrix} \frac{2\rho}{\delta t} + \rho B^n & 0 \\ 0 & 0 \end{bmatrix} \begin{pmatrix} \mathbf{u}^n \\ 0 \end{pmatrix} + \begin{bmatrix} f^{n+\frac{1}{2}} \\ 0 \end{bmatrix}. \tag{4.61}$$

with the inverse of the linear operator given by

$$\mathcal{A}^{-1} = \begin{bmatrix} \mathbf{I} & -\frac{\delta t}{2\rho}\nabla \\ 0 & \mathbf{I} - \frac{\delta t}{\rho}\frac{\eta}{2}\Delta \end{bmatrix} \begin{bmatrix} \mathbf{I} & 0 \\ 0 & -\Delta^{-1} \end{bmatrix} \begin{bmatrix} \mathbf{I} & 0 \\ -\frac{2\rho}{\delta t}\nabla \cdot & -\frac{\rho}{\delta t} \end{bmatrix} \begin{bmatrix} \left(\frac{2\rho}{\delta t} - \eta\Delta + \rho B^{n+1}\right)^{-1} & 0 \\ 0 & \mathbf{I} \end{bmatrix}. \tag{4.62}$$

In other words, the operator in (4.62) is a good preconditioner. Since the inverse of B^{n+1} is non-trivial, we use the following operator

$$\begin{bmatrix} \mathbf{I} & -\frac{\delta t}{2\rho}\nabla \\ 0 & \mathbf{I} - \frac{\delta t}{\rho}\frac{\eta}{2}\Delta \end{bmatrix} \begin{bmatrix} \mathbf{I} & 0 \\ 0 & -\Delta^{-1} \end{bmatrix} \begin{bmatrix} \mathbf{I} & 0 \\ -\frac{2\rho}{\delta t}\nabla \cdot & -\frac{\rho}{\delta t} \end{bmatrix} \begin{bmatrix} \left(\frac{2\rho}{\delta t} - \eta\Delta\right)^{-1} & 0 \\ 0 & \mathbf{I} \end{bmatrix}. \tag{4.63}$$

as the preconditioner for solving the Navier-Stokes equations in Step 1 and Step 3 of schemes 4.4 and 4.5. And it turns out to be effective numerically.

4.4.2 Velocity projection to decouple the Navier-Stokes equation

In our second approach, we can further decouple the velocity and pressure fields in Step 1 and Step 3 of schemes 4.4 and 4.5, using the classical velocity projection method. The energy stability still holds. Specifically, for the CN scheme of the NS equation, we can introduce the projection strategy by solving several Poisson-type equations sequentially. The corresponding energy law can also be derived. The equation (4.54) can be approximated by the following two steps with second-order accuracy.

- Step 1: solve the intermediate velocity field

$$\rho\frac{\tilde{\mathbf{u}}^{n+1}-\mathbf{u}^n}{\delta t}+\rho B(\overline{\mathbf{u}}^{n+\frac{1}{2}},\tilde{\mathbf{u}}^{n+\frac{1}{2}})=-\nabla p^n+\eta\Delta\tilde{\mathbf{u}}^{n+\frac{1}{2}}+f^{n+\frac{1}{2}}. \tag{4.64}$$

- Step 2: update the velocity field

$$\frac{\rho}{\delta t}(\mathbf{u}^{n+1}-\tilde{\mathbf{u}}^{n+1})=-\tfrac{1}{2}\nabla(p^{n+1}-p^n).$$
$$\nabla\cdot\mathbf{u}^{n+1}=0. \tag{4.65}$$

This leads to a new variant of second-order decoupled numerical schemes for the CHNS system.

Scheme 4.6. Given $(\mathbf{u}^n,\phi^n)$ and $(\mathbf{u}^{n-1},\phi^{n-1})$, we can obtain $(\mathbf{u}^{n+1},\phi^{n+1})$ in the following three steps:

- Step 1: in $[t_n,t_{n+\frac{1}{2}}]$, we set $\phi_\star=\phi^n$ and solve $\mathbf{u}_\star$ via the following three sub-steps.

  - Step 1.1, get $\tilde{\mathbf{u}}_\star$ from

$$\rho\frac{\tilde{\mathbf{u}}_\star-\mathbf{u}^n}{\delta t/2}+B(\overline{\mathbf{u}}^{n+\frac{1}{4}},\frac{\mathbf{u}_\star+\mathbf{u}^n}{2})=-\nabla p^n+\eta\Delta\frac{\tilde{\mathbf{u}}_\star+\mathbf{u}^n}{2}, \tag{4.66a}$$
$$\tilde{\mathbf{u}}_\star=0,\quad\text{on }\partial\Omega. \tag{4.66b}$$

  - Step 1.2, get $p_\star$ from

$$\Delta p_\star=\frac{4\rho}{\delta t}\nabla\cdot\tilde{\mathbf{u}}_\star+\Delta p^n, \tag{4.67a}$$
$$\nabla p_\star\cdot\mathbf{n}=0,\text{ on }\partial\Omega. \tag{4.67b}$$

  - Step 1.3, get $\mathbf{u}_\star$ from

$$\mathbf{u}_\star=\tilde{\mathbf{u}}_\star-\frac{\delta t}{4\rho}\nabla(p_\star-p^n). \tag{4.68}$$

- Step 2, in $[t_n,t_{n+1}]$, we solve $(\mathbf{u}_{\star\star},\phi_{\star\star})$ via two sub-steps.

  - Step 2.1, solve $(\phi_{\star\star},p)$ via the following system

$$\frac{\phi_{\star\star}-\phi_\star}{\delta t}+\nabla\cdot(\mathbf{u}_\star\overline{\phi}^{n+\frac{1}{2}})=\nabla\cdot((M(\overline{\phi}^{n+\frac{1}{2}})+\frac{\delta t(\overline{\phi}^{n+\frac{1}{2}})^2}{2\rho})\nabla\mu^{n+\frac{1}{2}})+\nabla\cdot(\frac{\delta t\overline{\phi}^{n+\frac{1}{2}}}{2\rho}\nabla p), \tag{4.69a}$$
$$\mu^{n+\frac{1}{2}}=-\frac{\gamma\varepsilon}{2}(\Delta\phi_{\star\star}+\Delta\phi_\star)+\frac{\gamma}{\varepsilon}\frac{\delta f}{\delta(\phi_\star,\phi_{\star\star})}, \tag{4.69b}$$
$$-\Delta p-\nabla\cdot(\overline{\phi}^{n+\frac{1}{2}}\nabla\mu^{n+\frac{1}{2}})=0, \tag{4.69c}$$
$$\nabla\mu^{n+\frac{3}{4}}\cdot\mathbf{n}=0,\quad\nabla\phi_{\star\star}\cdot\mathbf{n}=0,\quad\nabla p\cdot\mathbf{n}=0,\quad\text{on }\partial\Omega. \tag{4.69d}$$

  - Step 2.2, update $\mathbf{u}_{\star\star}$ via

$$\mathbf{u}_{\star\star}=\mathbf{u}_\star-\frac{\delta t}{\rho}(\nabla p+\overline{\phi}^{n+\frac{1}{2}}\nabla\mu^{n+\frac{1}{2}}). \tag{4.70}$$

- Step 3, in $[t_{n+\frac{1}{2}},t_{n+1}]$, we set $\phi^{n+1}=\phi_{\star\star}$, and solve $\mathbf{u}^{n+1}$ via the follow three sub-steps.

– Step 3.1, get $\tilde{\mathbf{u}}^{n+1}$ from

$$\rho\frac{\tilde{\mathbf{u}}^{n+1}-\mathbf{u}_{\star\star}}{\delta t/2}+B(\bar{\mathbf{u}}^{n+\frac{3}{4}},\frac{\tilde{\mathbf{u}}^{n+1}+\mathbf{u}_{\star\star}}{2})=-\nabla p_{\star}+\eta\Delta\frac{\mathbf{u}_{\star\star}+\tilde{\mathbf{u}}^{n+1}}{2}, \tag{4.71a}$$

$$\tilde{\mathbf{u}}^{n+1}=0 \quad \text{on } \partial\Omega. \tag{4.71b}$$

– Step 3.2, get p^{n+1} from

$$\Delta p^{n+1}=\frac{4\rho}{\delta t}\nabla\cdot\tilde{\mathbf{u}}^{n+1}+\Delta p_{\star}, \tag{4.72a}$$

$$\nabla p^{n+1}\cdot\mathbf{n}=0, \text{ on } \partial\Omega. \tag{4.72b}$$

– Step 3.3, get $\mathbf{u}^{n+1}$ from

$$\mathbf{u}^{n+1}=\tilde{\mathbf{u}}^{n+1}-\frac{\delta t}{4\rho}\nabla(p^{n+1}-p_{\star}). \tag{4.73}$$

Remark 4.7. Note the decoupled steps in (4.67a)-(4.68) are from the general scheme

$$\frac{\rho}{\delta t/2}(\mathbf{u}_{\star}-\tilde{\mathbf{u}}_{\star})=-\frac{1}{2}(\nabla p_{\star}-\nabla p^{n}). \tag{4.74}$$

Similarly, the steps in (4.72a)-(4.73) are from the general scheme

$$\frac{\rho}{\delta t/2}(\mathbf{u}^{n+1}-\tilde{\mathbf{u}}_{\star\star})=-\frac{1}{2}(\nabla p^{n+1}-\nabla p_{\star}). \tag{4.75}$$

Remark 4.8. We further comment on Step 2. Based on the operator splitting strategy, in $[t_n,t_{n+1}]$, we solve $(\mathbf{u}_{\star\star},\phi_{\star\star})$ via

$$\rho\frac{\mathbf{u}_{\star\star}-\mathbf{u}_{\star}}{\delta t}=-\nabla p-\bar{\phi}^{n+\frac{1}{2}}\nabla\mu^{n+\frac{1}{2}}, \tag{4.76a}$$

$$\mu^{n+\frac{1}{2}}=-\frac{\gamma\varepsilon}{2}(\Delta\phi_{\star\star}+\Delta\phi_{\star})+\frac{\gamma}{\varepsilon}\frac{\delta f}{\delta(\phi_{\star},\phi_{\star\star})}, \tag{4.76b}$$

$$\nabla\cdot\frac{\mathbf{u}_{\star\star}+\mathbf{u}_{\star}}{2}=0, \tag{4.76c}$$

$$\frac{\phi_{\star\star}-\phi_{\star}}{\delta t}=-\nabla\cdot(\frac{\mathbf{u}_{\star\star}+\mathbf{u}_{\star}}{2}\bar{\phi}^{n+\frac{1}{2}})+\nabla\cdot(M(\overline{\phi}^{n+\frac{1}{2}})\nabla\mu^{n+\frac{1}{2}}), \tag{4.76d}$$

$$\nabla\mu^{n+\frac{1}{2}}\cdot\mathbf{n}=0, \quad \nabla\phi_{\star\star}\cdot\mathbf{n}=0, \quad \mathbf{u}_{\star\star}=0, \quad \text{on } \partial\Omega. \tag{4.76e}$$

Decoupling the velocity field from the phase variables, we can simplify (4.76) into the equations (4.69)-(4.70).

Besides, we still have the energy stability of this scheme as below.

Theorem 4.3. *The decoupled scheme 4.6 is energy stable in the sense that*

$$\hat{\mathcal{E}}(\mathbf{u}^{n+1},p^{n+1},\phi^{n+1})-\hat{\mathcal{E}}(\mathbf{u}^{n},p^{n},\phi^{n})\leq$$
$$-\frac{\delta t}{2}\left[\eta\|\nabla\frac{\mathbf{u}_{\star}+\mathbf{u}^{n}}{2}\|^{2}+\eta\|\nabla\frac{\mathbf{u}^{n+1}+\mathbf{u}_{\star\star}}{2}\|^{2}+2\|\sqrt{M(\overline{\phi}^{n+\frac{1}{2}})}\nabla\mu^{n+\frac{1}{2}}\|^{2}\right], \tag{4.77}$$

where the modified energy is defined as $\hat{\mathcal{E}}(\mathbf{u},p,\phi)=E(\mathbf{u})+\tilde{E}(\nabla p)+F(\phi)$, with the three terms specified as

$$E(\mathbf{u})=\int_{\Omega}\frac{\rho}{2}|\mathbf{u}|^{2}d\mathbf{x}, \quad \tilde{E}(\nabla p)=\int_{\Omega}\frac{\delta t^{2}}{32\rho}|\nabla p|^{2}d\mathbf{x}, \quad F(\phi)=\gamma\int_{\Omega}\frac{\varepsilon}{2}|\nabla\phi|^{2}+\frac{1}{\varepsilon}f(\phi)d\mathbf{x}. \tag{4.78}$$

Proof. Since the proof of this theorem is a little different from the proofs of the other two theorems in previous sections, we will illustrate the details. First of all, we take the inner product of (4.66a) with $\frac{\delta t}{2}\frac{\tilde{\mathbf{u}}_{\star}+\mathbf{u}^{n}}{2}$, we obtain

$$\frac{\rho}{2}(\|\tilde{\mathbf{u}}_{\star}\|^{2}-\|\mathbf{u}^{n}\|^{2})=-\frac{\delta t}{2}(\nabla p^{n},\frac{\tilde{\mathbf{u}}_{\star}+\mathbf{u}^{n}}{2})-\frac{\delta t}{2}\eta\|\nabla\frac{\tilde{\mathbf{u}}_{\star}+\mathbf{u}^{n}}{2}\|^{2}. \tag{4.79}$$

If we take the inner product of (4.74) with $\delta t \mathbf{u}_\star$, we have

$$\frac{\rho}{2}(\|\mathbf{u}_\star\|^2 - \|\tilde{\mathbf{u}}_\star\|^2 + \|\mathbf{u}_\star - \tilde{\mathbf{u}}_\star\|^2) = 0. \tag{4.80}$$

We can rewrite (4.74) as

$$\frac{\rho}{\delta t/2}(\mathbf{u}_\star + \mathbf{u}^n - 2\frac{\mathbf{u}^n + \tilde{\mathbf{u}}_\star}{2}) + \frac{1}{2}(\nabla p_\star - \nabla p^n) = 0. \tag{4.81}$$

and test it with $\frac{\delta t^2}{8\rho}\nabla p^n$. It yields

$$-\frac{\delta t}{2}(\frac{\tilde{\mathbf{u}}_\star + \mathbf{u}^n}{2}, \nabla p^n) + \frac{\delta t^2}{32\rho}(\|\nabla p_\star\|^2 - \|\nabla p^n\|^2 - \|\nabla(p_\star - p^n)\|^2) = 0. \tag{4.82}$$

Taking the inner product of (4.74) with itself, we have

$$\frac{\delta t^2}{32\rho}\|\nabla(p_\star - p^n)\|^2 - \frac{\rho}{2}\|\mathbf{u}_\star - \tilde{\mathbf{u}}_\star\|^2 = 0. \tag{4.83}$$

Adding the equations (4.79),(4.80), (4.82) and (4.83) together will give us

$$(\frac{\rho}{2}\|\mathbf{u}_\star\|^2 + \frac{\delta t^2}{32\rho}\|\nabla p_\star\|^2) - (\frac{\rho}{2}\|\mathbf{u}^n\|^2 + \frac{\delta t^2}{32\rho}\|\nabla p^n\|^2) = -\frac{\delta t}{2}\eta\|\nabla\frac{\tilde{\mathbf{u}}_\star + \mathbf{u}^n}{2}\|^2. \tag{4.84}$$

Take inner product of (4.76a) with $\delta t\frac{\mathbf{u}_{\star\star} + \mathbf{u}_\star}{2}$, we have

$$\frac{\rho}{2}(\|\mathbf{u}_{\star\star}\|^2 - \|\mathbf{u}_\star\|^2) = -\delta t(\frac{\mathbf{u}_{\star\star} + \mathbf{u}_\star}{2}\overline{\phi}^{n+\frac{1}{2}}\nabla\mu^{n+\frac{1}{2}}). \tag{4.85}$$

If we take inner product of (4.76c) with $\delta t\mu^{n+\frac{1}{2}}$, and (4.76d) with $\delta t(\phi_{\star\star} - \phi_\star)$, we have

$$F(\phi_{\star\star}) - F(\phi_\star) = -\delta t(\nabla\cdot(\frac{\mathbf{u}_{\star\star} + \mathbf{u}_\star}{2}\overline{\phi}^{n+\frac{1}{2}}), \mu^{n+\frac{1}{2}}) - \delta t\|\sqrt{M(\overline{\phi}^{n+\frac{1}{2}})}\nabla\mu^{n+\frac{1}{2}}\|^2. \tag{4.86}$$

Adding the equations (4.85) and (4.86) above, we have

$$\frac{\rho}{2}(\|\mathbf{u}_{\star\star}\|^2 - \|\mathbf{u}_\star\|^2) + F(\phi_{\star\star}) - F(\phi_\star) = -\delta t\|\sqrt{M(\overline{\phi}^{n+\frac{1}{2}})}\nabla\mu^{n+\frac{1}{2}}\|^2. \tag{4.87}$$

Similarly, from (4.71a)-(4.72b), we will obtain

$$(\frac{\rho}{2}\|\mathbf{u}^{n+1}]\|^2 + \frac{\delta t^2}{32\rho}\|\nabla p^{n+1}]\|^2) - (\frac{\rho}{2}\|\mathbf{u}_{\star\star}\|^2 + \frac{\delta t^2}{32\rho}\|\nabla p_\star\|^2) = -\frac{\delta t}{2}\eta\|\nabla\frac{\tilde{\mathbf{u}}^{n+1} + \mathbf{u}_{\star\star}}{2}\|^2. \tag{4.88}$$

Adding the equations (4.84), (4.87) and (4.88), it lead to

$$(\frac{\rho}{2}\|\mathbf{u}^{n+1}\|^2 + \frac{\delta t^2}{32\rho}\|\nabla p^{n+1}]\|^2 + F(\phi^{n+1})) - (\frac{\rho}{2}\|\mathbf{u}^n\|^2 + \frac{\delta t^2}{32\rho}\|\nabla p^n\|^2 + F(\phi^n))$$
$$= -\frac{\delta t}{2}\left[\eta\|\nabla\frac{\tilde{\mathbf{u}}^{n+1} + \mathbf{u}_{\star\star}}{2}\|^2 + \eta\|\nabla\frac{\tilde{\mathbf{u}}_{\star\star} + \mathbf{u}^n}{2}\|^2 + \|\sqrt{M(\overline{\phi}^{n+\frac{1}{2}})}\nabla\mu^{n+\frac{1}{2}}\|^2\right]. \tag{4.89}$$

$\square$

Remark 4.9. We note that the modified free energy $\hat{\mathcal{E}}$ is a second-order perturbation of the original energy. This type of perturbation is preferred than the modified free energy with auxiliary variables since its errors are explicitly written as $\tilde{E}(\nabla p)$, which is $O(\delta t^2)$.

4.5 A completely decoupled scheme based on Strang splitting and pressure correction

In this section, we combine the idea of Strang splitting with that of pressure correction to design a time-split method in which the velocity field, the pressure, and the phase field variable are computed independent of each other. This leads to a new variant of second-order decoupled numerical schemes for the CHNS system in (1.3)-(1.4).

Scheme 4.7. Given $(\mathbf{u}^n, p^n, \phi^n)$ and $(\mathbf{u}^{n-1}, \phi^{n-1})$, we obtain $(\mathbf{u}^{n+1}, p^{n+1}, \phi^{n+1})$ in the following three steps:

- Step 1: in $[t_n, t_{n+\frac{1}{2}}]$, we solve for the intermediate variables $(\phi_\star, \mathbf{u}_\star, p_\star)$ via

  - Step 1.1, solve for $\phi_\star$ via the following system

  $$\frac{1}{\delta t/2}(\phi_\star - \phi^n) + \nabla \cdot (\mathbf{u}^n \overline{\phi}^{n+\frac{1}{4}}) = \nabla \cdot (\frac{\delta t}{4\rho}(\overline{\phi}^{n+\frac{1}{4}})^2 \nabla \mu^{n+\frac{1}{4}}) + \frac{\delta t}{4\rho} \nabla \cdot (\overline{\phi}^{n+\frac{1}{4}} \nabla p^n), \tag{4.90a}$$

  $$\mu^{n+\frac{1}{4}} = -\frac{\gamma\varepsilon}{2}(\Delta\phi_\star + \Delta\phi^n) + \frac{\gamma}{\varepsilon}\frac{\delta f}{\delta(\phi^n, \phi_\star)}, \tag{4.90b}$$

  $$\nabla\mu^{n+\frac{1}{4}}\cdot\mathbf{n} = 0, \quad \nabla\phi_\star\cdot\mathbf{n} = 0, \quad \text{on } \partial\Omega. \tag{4.90c}$$

  - Step 1.2, solve for q from the Poisson equation

  $$-\Delta q - \nabla \cdot (\overline{\phi}^{n+\frac{1}{4}} \nabla\mu^{n+\frac{1}{4}}) = 0, \tag{4.91a}$$

  $$\nabla q \cdot \mathbf{n} = 0, \quad \text{on } \partial\Omega \tag{4.91b}$$

  - Step 1.3, update $(\mathbf{u}_\star, p_\star)$ via

  $$\mathbf{u}_\star = \mathbf{u}^n - \frac{\delta t}{2\rho}(\nabla q + \overline{\phi}^{n+\frac{1}{4}}\nabla\mu^{n+\frac{1}{4}}), \tag{4.92a}$$

  $$p_\star = 2q - p^n. \tag{4.92b}$$

- Step 2: in $[t_n, t_{n+1}]$, we solve for $(\mathbf{u}_{\star\star}, \phi_{\star\star})$ via two sub-steps.

  - Step 2.1: solve for $\mathbf{u}_{\star\star}$ via

  $$\rho\frac{\mathbf{u}_{\star\star} - \mathbf{u}_\star}{\delta t} + B(\overline{\mathbf{u}}^{n+\frac{1}{2}}, \frac{\mathbf{u}_{\star\star} + \mathbf{u}_\star}{2}) = \eta\Delta\frac{\mathbf{u}_{\star\star} + \mathbf{u}_\star}{2}, \tag{4.93a}$$

  $$\mathbf{u}_{\star\star} = 0, \quad \text{on } \partial\Omega. \tag{4.93b}$$

  - Step 2.2: solve for $\phi_{\star\star}$ via

  $$\frac{\phi_{\star\star} - \phi_\star}{\delta t} = \nabla \cdot (M(\overline{\phi}^{n+\frac{1}{2}})\nabla\mu^{n+\frac{1}{2}}), \tag{4.94a}$$

  $$\mu^{n+\frac{1}{2}} = -\frac{\gamma\varepsilon}{2}(\Delta\phi_{\star\star} + \Delta\phi_\star) + \frac{\delta f}{\delta(\phi_\star, \phi_{\star\star})}, \tag{4.94b}$$

  $$\nabla\mu^{n+\frac{1}{2}}\cdot\mathbf{n} = 0, \quad \nabla\phi_{\star\star}\cdot\mathbf{n} = 0, \quad \text{on } \partial\Omega. \tag{4.94c}$$

- Step 3, in $[t_{n+\frac{1}{2}}, t_{n+1}]$, we solve for $(\mathbf{u}^{n+1}, p^{n+1}, \phi^{n+1})$ via the follow three sub-steps.

  - Step 3.1, solve for ϕ^{n+1} via the following system

  $$\frac{1}{\delta t/2}(\phi^{n+1} - \phi_{\star\star}) + \nabla \cdot (\mathbf{u}_{\star\star}\overline{\phi}^{n+\frac{3}{4}}) = \nabla \cdot (\frac{\delta t}{4\rho}(\overline{\phi}^{n+\frac{3}{4}})^2\nabla\mu^{n+\frac{3}{4}}) + \frac{\delta t}{4\rho}\nabla \cdot (\overline{\phi}^{n+\frac{3}{4}}\nabla p_\star), \tag{4.95a}$$

  $$\mu^{n+\frac{3}{4}} = -\frac{\gamma\varepsilon}{2}(\Delta\phi_{\star\star} + \Delta\phi^{n+1}) + \frac{\gamma}{\varepsilon}\frac{\delta f}{\delta(\phi_{\star\star}, \phi^{n+1})}, \tag{4.95b}$$

  $$\nabla\mu^{n+\frac{3}{4}}\cdot\mathbf{n} = 0, \quad \nabla\phi^{n+1}\cdot\mathbf{n} = 0, \quad \text{on } \partial\Omega. \tag{4.95c}$$

– Step 3.2, solve for q from the Poisson equation

$$-\Delta q - \nabla \cdot (\overline{\phi}^{n+\frac{3}{4}} \nabla \mu^{n+\frac{3}{4}}) = 0, \tag{4.96a}$$

$$\nabla q \cdot \mathbf{n} = 0, \quad \text{on } \partial\Omega \tag{4.96b}$$

– Step 3.3, update $(\mathbf{u}_{n+1}, p_{n+1})$ via

$$\mathbf{u}^{n+1} = \mathbf{u}_{\star\star} - \frac{\delta t}{2\rho}(\nabla q + \overline{\phi}^{n+\frac{3}{4}} \nabla \mu^{n+\frac{3}{4}}), \tag{4.97a}$$

$$p^{n+1} = 2q - p_\star. \tag{4.97b}$$

Similarly, by introducing another intermediate velocity

$$\tilde{\mathbf{u}}_\star = \mathbf{u}^n - \frac{\delta t}{2\rho}(\nabla p^n + \overline{\phi}^{n+\frac{1}{4}} \nabla \mu^{n+\frac{1}{4}}), \tag{4.98}$$

the scheme (4.90)–(4.92) can be equivalently written as

$$\frac{1}{\delta t/2}(\phi_\star - \phi^n) + \nabla \cdot (\frac{\tilde{\mathbf{u}}_\star + \mathbf{u}^n}{2} \overline{\phi}^{n+\frac{1}{4}}) = 0, \tag{4.99a}$$

$$\mu^{n+\frac{1}{4}} = -\frac{\gamma\varepsilon}{2}(\Delta\phi_\star + \Delta\phi^n) + \frac{\gamma}{\varepsilon}\frac{\delta f}{\delta(\phi^n, \phi_\star)}, \tag{4.99b}$$

$$\rho\frac{\mathbf{u}_\star - \mathbf{u}^n}{\delta t/2} + \frac{1}{2}(\nabla p^n + \nabla p_\star) = -\overline{\phi}^{n+\frac{1}{4}} \nabla \mu^{n+\frac{1}{4}}, \quad \nabla \cdot \mathbf{u}_\star = 0, \tag{4.99c}$$

$$\nabla \mu^{n+\frac{1}{4}} \cdot \mathbf{n} = 0, \quad \nabla\phi_\star \cdot \mathbf{n} = 0, \quad \mathbf{u}_\star \cdot \mathbf{n} = 0, \quad \text{on } \partial\Omega. \tag{4.99d}$$

Likewise, the scheme (4.95)–(4.97) can be similarly expressed in an equivalent form.

The fully decoupled time-marching scheme satisfies an energy law.

Theorem 4.4. *The decoupled scheme 4.7 is energy stable in the sense that*

$$\hat{\mathcal{E}}(\mathbf{u}^{n+1}, p^{n+1}, \phi^{n+1}) - \hat{\mathcal{E}}(\mathbf{u}^n, p^n, \phi^n) = -\delta t\left[\eta\|\nabla\frac{\mathbf{u}_{\star\star} + \mathbf{u}_\star}{2}\|^2 + \|\sqrt{M(\overline{\phi}^{n+\frac{1}{2}})}\nabla\mu^{n+\frac{1}{2}}\|^2\right], \tag{4.100}$$

where the modified energy is defined as $\hat{\mathcal{E}}(\mathbf{u}, p, \phi) = E(\mathbf{u}) + \tilde{E}(\nabla p) + F(\phi)$, with the three terms specified as

$$E(\mathbf{u}) = \int_\Omega \frac{\rho}{2}|\mathbf{u}|^2 d\mathbf{x}, \quad \tilde{E}(\nabla p) = \int_\Omega \frac{\delta t^2}{32\rho}|\nabla p|^2 d\mathbf{x}, \quad F(\phi) = \gamma\int_\Omega \frac{\varepsilon}{2}|\nabla\phi|^2 + \frac{1}{\varepsilon}f(\phi)d\mathbf{x}. \tag{4.101}$$

Proof. The proof is largely the same as the proof for Theorem 4.3. We omit the details for brevity. □

5 Numerical Results

The central finite difference on staggered grids for the spatial discretization and the operator splitting finite difference method in uniform time meshes for the temporal discretization are independent. Thus, the full discrete schemes for the CHNS system can be easily obtained by literately combine the spatial discretization in Section 3 and temporal discretization in Section 4. Here we won't elaborate on the details for simplicity. In this section, we conduct several numerical experiments with the proposed schemes.

5.1 Time step refinement tests

First of all, we verify that the proposed numerical algorithms are second-order in time indeed. Consider a square domain $\Omega = [0, L_x] \times [0, L_y]$ with $L_x = L_y = 1$. We fix the parameters $\rho = 1$, $\eta = 1.0$, $M = 0.01$, $\varepsilon = 0.01$, $\gamma = 0.01$. The initial profiles are chosen as

$$\mathbf{u}(t=0) = 0, \quad \phi(t=0) = \tanh\frac{R - \sqrt{(x - 0.5L_x)^2 + 2*(y - 0.5L_y)^2}}{2\varepsilon}, \text{ with } R = 0.2.$$
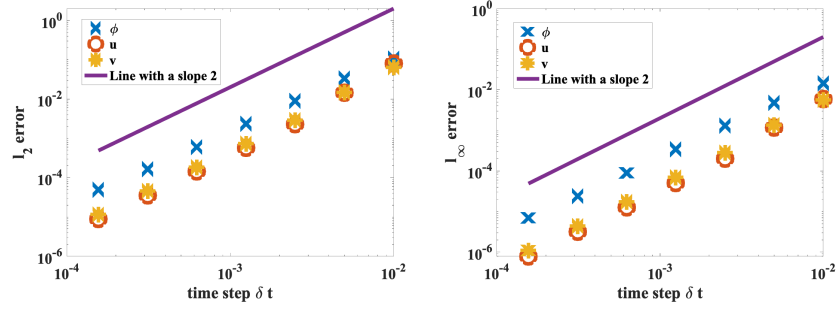
Figure 5.1: Temporal mesh refinement test for scheme 4.4. Here both the L^2 errors and L^∞ errors using different time step sizes are shown. We observe that the scheme 4.4 provides 2nd-order temporal accuracy.
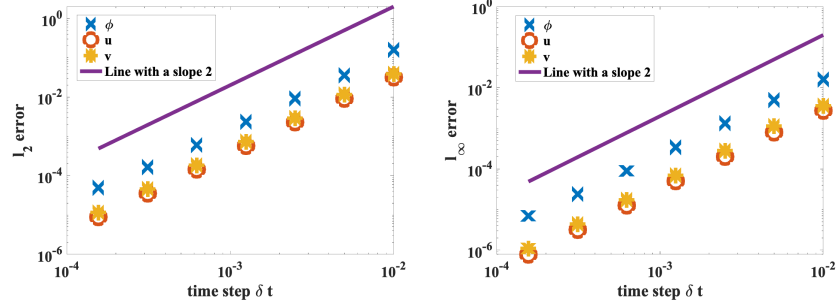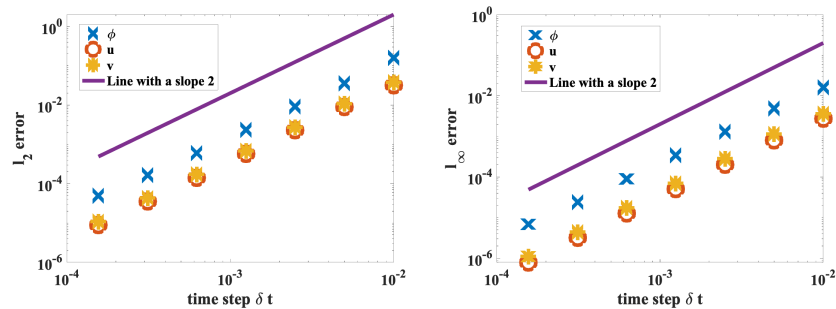

Figure 5.2: Temporal mesh refinement test for scheme 4.5. Here both the L^2 errors and L^∞ errors using different time step sizes are shown. We observe that the scheme 4.5 provides 2nd-order temporal accuracy.

We use the meshes $N_x = N_y = 128$, and numerical solutions with various time steps are calculated. Since the true solution is unknown, we calculate the errors at $T = 0.2$ as the differences between two numerical solutions with adjacent time step sizes. The three proposed numerical schemes 4.4, 4.5, 4.6 are tested with the numerical results summarized in Figure 5.1, 5.2 and 5.3, respectively. It can be easily seen that all the three proposed schemes reach second-order accuracy in time when the time step is small.

In addition, it seems that the three schemes provide similar numerical results and accuracy, given they are using the same time steps. This is no surprise since the three schemes only differ slightly, and the major numerical errors resulted from these three schemes are due to the operator splitting. Acknowledging this fact, we use scheme 4.6 for all numerical simulations in the rest of this paper.

5.2 Spatial mesh refinement test

Next, we conduct the spatial mesh refinement test for the scheme 4.6. We use the same parameters and initial conditions as the examples above, and we use a fine time step $\delta t = 10^{-4}$ to eliminate the possible effects of temporal errors on the spatial mesh tests. Various mesh sizes $N_x = N_y = N$, with $N = 64 \times (2k+1)$, $k = 0,1,2,3,4,5,6$, are used. Given that we are using staggered grids for spatial

Figure 5.3: Temporal mesh refinement test for scheme 4.6. Here both the L^2 errors and L^∞ errors using different time step sizes are shown. We observe that the scheme 4.6 provides 2nd-order temporal accuracy.

discretization, these mesh grids choices would ensure all the cases have numerical solutions on the coarse grid $N = 64$. So the errors between adjacent numerical solutions on the coarse grid $N = 64$ at $T = 0.2$ are calculated. The results are summarized in Table 5.1, where we observe a second-order spatial convergence.

Table 5.1: Spatial mesh refinement test

	ϕ		u		v	
N	L^2-error	Order	L^2-error	Order	L^2-error	Order
64	–	–	–	–	–	–
192	0.6397	–	0.001381	–	0.001549	–
320	0.02646	2.63	0.0001007	2.09	0.00007986	2.43
448	0.007039	2.06	0.00002719	2.05	0.00002159	2.04
576	0.002867	2.02	0.00001111	2.02	0.000008827	2.02
704	0.001445	2.01	0.000005610	2.01	0.000004457	2.01
832	0.0008289	2.01	0.000003222	2.01	0.000002560	2.01

5.3 Bubbles merging driven by surface tension

Next, we conduct several numerical simulations on the merging of the two bubbles that is driven by surface tension. We follow the similar set up as in [19]. Consider the domain $\Omega = [0, L_x] \times [0, L_y]$, with $L_x = L_y = 1$. The initial conditions are provided as $\mathbf{u}(x, y, t = 0) = \mathbf{0}$, and

$$\phi(x, y, t = 0) = 1 - \tanh \frac{-r + \sqrt{(x - x_a)^2 + (y - y_a)^2}}{2\varepsilon} - \tanh \frac{-r + \sqrt{(x - x_b)^2 + (y - y_b)^2}}{2\varepsilon}.$$

with $x_a = 0.5L_x - \frac{r}{\sqrt{2}}$, $y_a = 0.5L_y + \frac{r}{\sqrt{2}}$, $x_b = 0.5L_x + \frac{r}{\sqrt{2}}$, $y_b = 0.5L_y - \frac{r}{\sqrt{2}}$, $r = 0.15$. The parameters are chosen as $\rho = 1$, $M = 0.01$, $\gamma = 0.01$, $\varepsilon = 0.01$, and we use uniform meshes $N_x = N_y = 128$ and $\delta t = 10^{-3}$. The numerical results with viscosity $\eta = 0.01$ are shown in Figure 5.4, where the profiles of the phase variable ϕ at various times are shown. It can be observed that the two drops merge into a single drop.

As a comparison, we present another simulation with the same parameters and other settings, except a smaller viscosity $\eta = 0.001$. The profiles of the phase variables at the same times as the previous example are summarized in Figure 5.5. Though the two bubbles eventually merged into a single one and the round drop reaches a steady state, the dynamics between Figure 5.4 and 5.5 are dramatically different. Mainly, when the viscosity is small, the effect of inertia is not negligible anymore. In Figure 5.5, we observe that the drop squeezed and then stretched, showing back-and-forth damping oscillations (due to the exchanges between the kinetic energy and the Helmholtz free energy). And it eventually stabilizes as a round drop. In other words, the hydrodynamics or the Navier-Stokes equation shall not be ignored when the inertia has noticeable effects on the dynamics.

To further compare the dynamics for the two cases above, we also visualize the velocity fields for both cases, with the results summarized in Figure 5.6. It can be shown that the kinetic energy is high for the case with smaller viscosity, and the kinetic energy shows oscillating and damping dynamics (by noticing the magnitude of the velocity field is decreasing with time).

Meanwhile, as a double-verification of the energy stable property of our proposed scheme 4.6, the energy evolution with time for both cases are summarized in Figure 5.7. We can observe that the energy is dissipating in time for both cases. The one with smaller viscosity is dissipating slower, which is reasonable, as the dissipation rate is proportional to the viscosity as shown in 1.5.
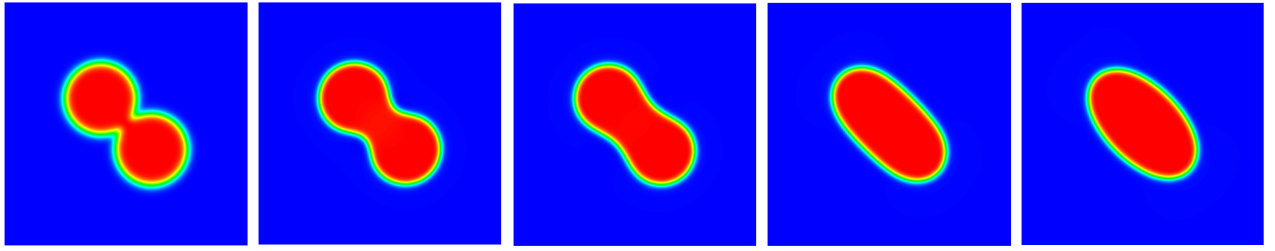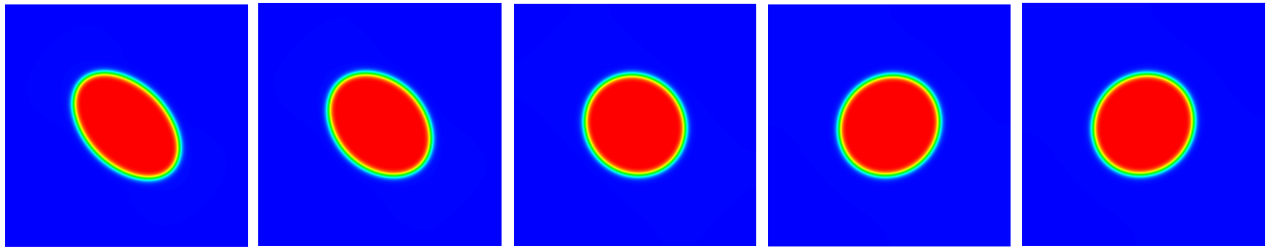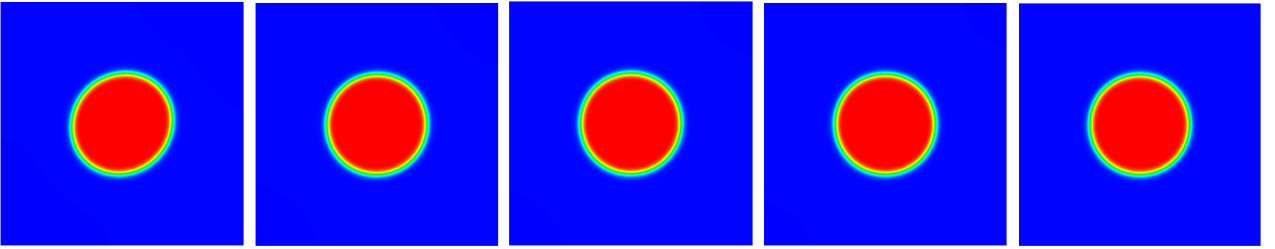
(a) ϕ at $t=0,0.2,0.4,0.8,1.0$

(b) ϕ at $t=1.2,1.5,2,3,3.2$

(c) ϕ at $t=3.4,4.6,4.8,5,10$

Figure 5.4: The dynamics of bubble merging under hydrodynamic environment with viscosity $\eta=0.01$. In this figure, the profiles of the phase variable ϕ are shown at time $t=0$, 0.2, 0.4, 0.8, 1.0, 1.2, 1.5, 2.0, 3.0, 3.2, 3.4, 4.6, 4.8, 5 and 10.
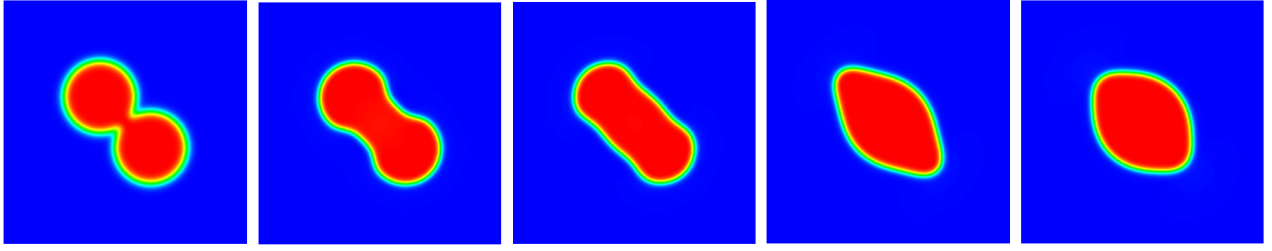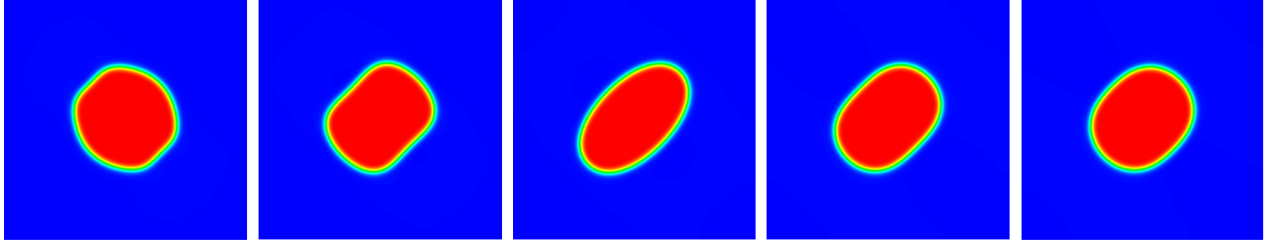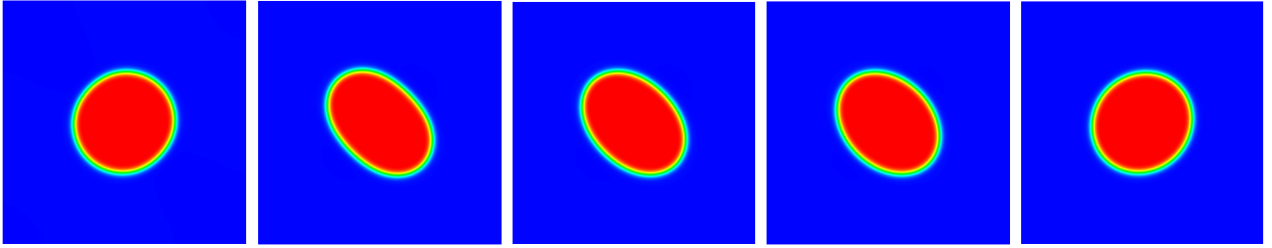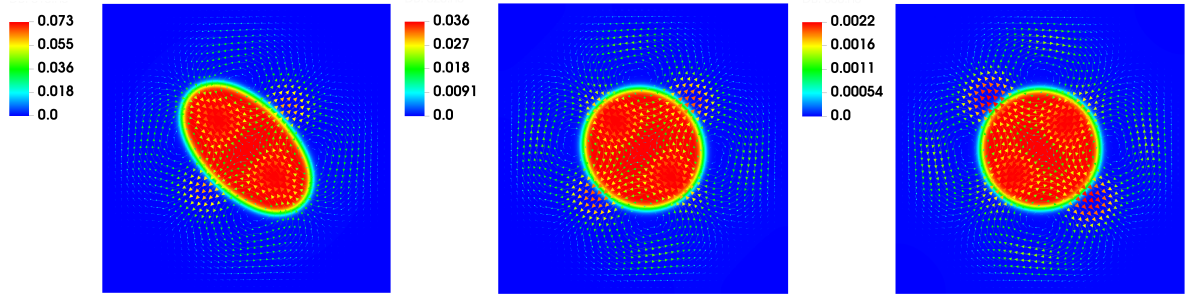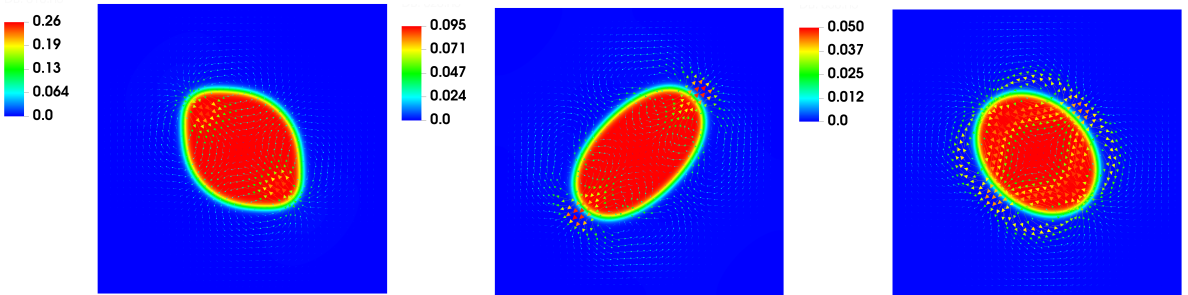
(a) ϕ at $t=0,0.2,0.4,0.8,1.0$

(b) ϕ at $t=1.2,1.5,2,3,3.2$

(c) ϕ at $t=3.4,4.6,4.8,5,10$

Figure 5.5: The dynamics of bubble merging under hydrodynamic environment with viscosity $\eta=0.001$. In this figure, the profiles of the phase variable ϕ are shown at different times.

(a) Velocity field for Figure 5.4 at time $t=1,2,5$

(b) Velocity field for Figure 5.5 at time $t=1,2,5$

Figure 5.6: Visualization of the velocity field for the dynamics in Figure 5.4 and 5.5. (a) the velocity field for Figure 5.4; (b) the velocity field for Figure 5.5.

(a) Energy evolution for Figure 5.4

(b) Energy evolution for Figure 5.5
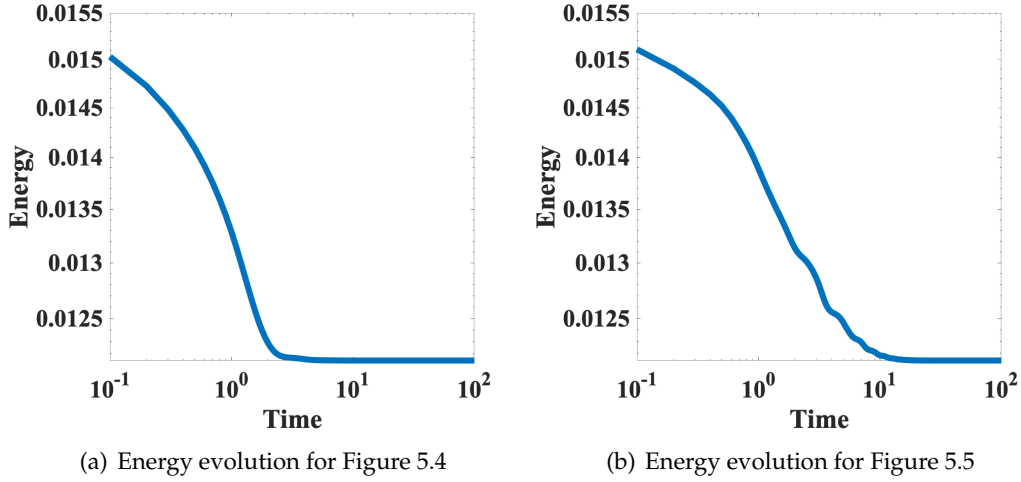
Figure 5.7: The time evolution of the energy in log-log scale.

5.4 Coarsening

Next, we investigate the coarsening dynamics under hydrodynamics environments. We use the domain $\Omega = [0,L_x] \times [0,L_y]$ with $L_x = 1$, $L_y = 2$. The parameters are picked as $\rho = 1$, $\eta = 1.0$, $M = 0.01$, $\varepsilon = 0.01$. To solve the problem, we use uniform meshes with $N_x = 128$ and $N_y = 256$ and $\delta t = 10^{-3}$. And we pick different values for the surface tension γ. Set a random initial condition for the phase variable $\phi(x,y,t=0) = 0.9(\frac{y}{L_y} - 0.5) + 0.001 * rand(-1,1)$, and $\mathbf{u}(x,y,t=0) = \mathbf{0}$. The numerical results with $\gamma = 0.1$ and $\gamma = 0.01$ are summarized in Figure 5.8. We observe that when the volume fraction of two phases is similar, saying in the middle of the domain, spinodal decomposition takes more effect. Meanwhile, when the volume fractions of each phase differ dramatically, the nucleation takes more effect.

Furthermore, the velocity fields for both cases are shown in Figure 5.9. We observe that the velocity field has a larger magnitude at the regions that are changing rapidly, which means the hydrodynamics (kinetic energy) is interacting with the surface tension (Helmholtz free energy).

Meanwhile, the energy evolution for both cases are summarized in Figure 5.10. We observe that the coarsening dynamics changes faster when the surface tension is high. This is agreeable with the energy dissipation rate in (1.5).

5.5 Ostwald ripening under hydrodynamics

In this example, we study the Ostwald ripening dynamics driven by the CHNS system. In particular, we are interested in how energy evolves under topological changes. We consider the domain $\Omega = [0,L_x] \times [0,L_y]$ with $L_x = L_y = 1$. We set the initial velocity as zero and the initial profile of ϕ as seven drops in various radii, a shown in Figure 5.11. We fix the parameters $M = 0.01$, $\varepsilon = 0.01$ and $\rho = 1$. Then we pick different viscosity η. The scheme 4.6 is used for this simulation with $\delta t = 10^{-3}$. The energy evolutions are summarized in Figure 5.11, where the Ostwald ripening dynamics take place. We observe that the energy changes rapidly when topological changes are happening.

5.6 Lid-driven cavity

In the last example, we simulate the lid-driven cavity problem using the CHNS system. The domain is set up as $\Omega = [0,L_x] \times [0,L_y]$ with $L_x = L_y = 1$, with shear on the top. This is related with the zero Dirichlet boundary condition for the velocity at the boundary, except at $y = L_y$ for which we propose $\mathbf{u}|_{y=L_y} = (1,0)$. We choose the initial condition for the phase variable $\phi(x,y,t=0) = \tanh\frac{R - \sqrt{(x-0.5L_x)^2 + (y-0.5L_y)^2}}{2\varepsilon}$, with $R = 0.15$. The boundary condition for the phase variable ϕ remains the same. We use the following parameters $\rho = 1$, $\eta = 1$, $M = 0.01$, $\varepsilon = 0.01$ and we use various surface tension parameter γ. We use mesh sizes $N_x = N_y = 128$ and $\delta t = 10^{-3}$. The profiles of ϕ at various times
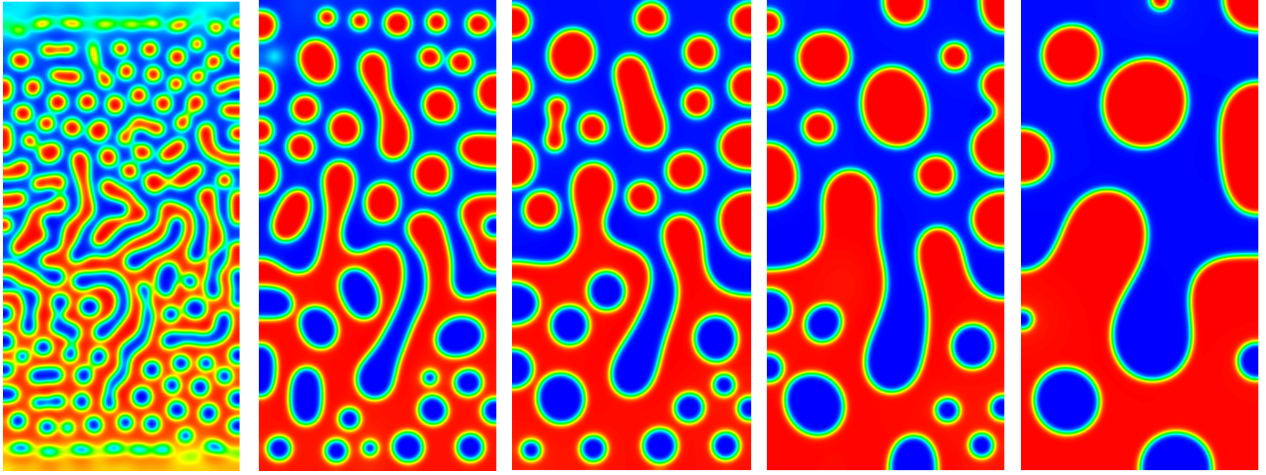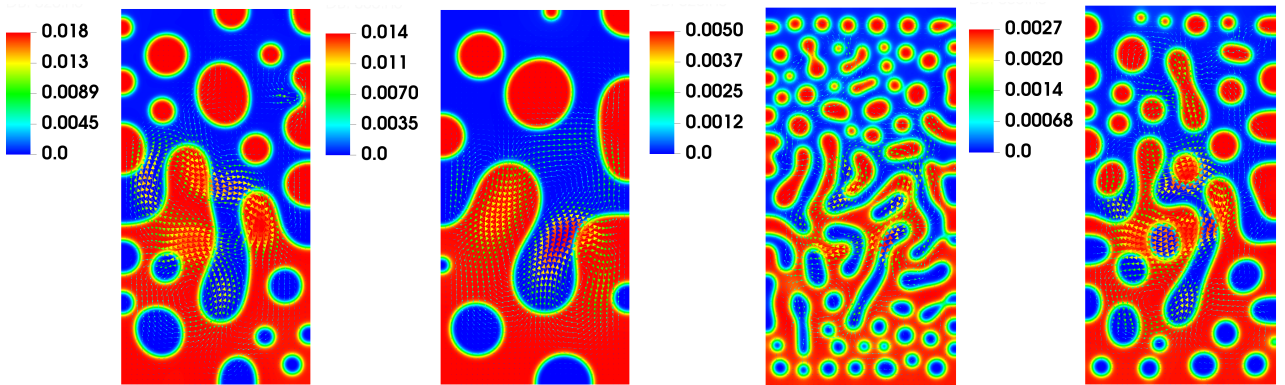
(a) ϕ at $t=0.1,0.5,1,2,6.5$ for the case $\gamma=0.1$
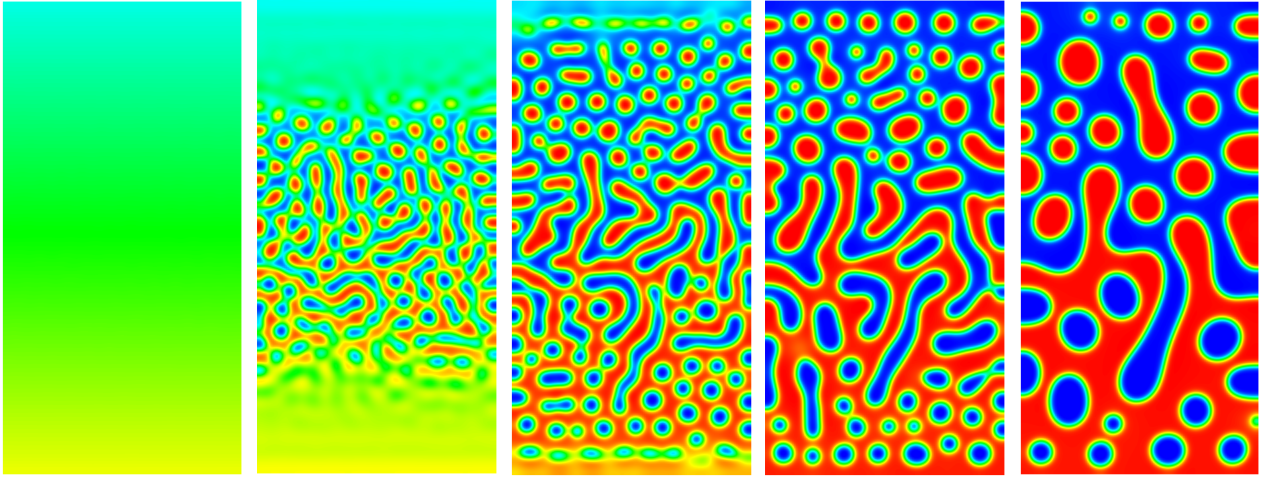
(b) ϕ at $t=0.1,0.5,1,2,6.5$ for the case $\gamma=0.01$

Figure 5.8: Time evolution of phase variables with different surface tension. In (a) the profiles of ϕ at various times are shown for the case $\gamma=0.1$; (b) the profiles of ϕ at various times are shown for the case $\gamma=0.01$.
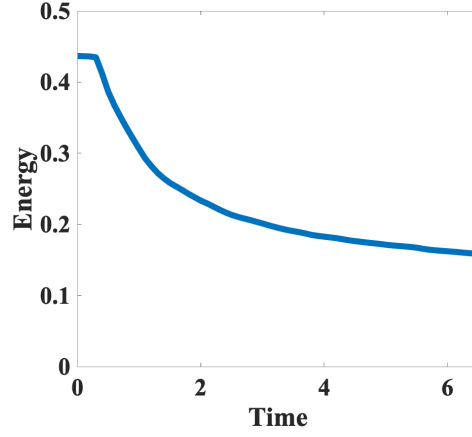

(a) velocity field at $t=2,6.5$ for Figure 5.8(a)

(b) velocity field at $t=2,6.5$ for Figure 5.8(b)

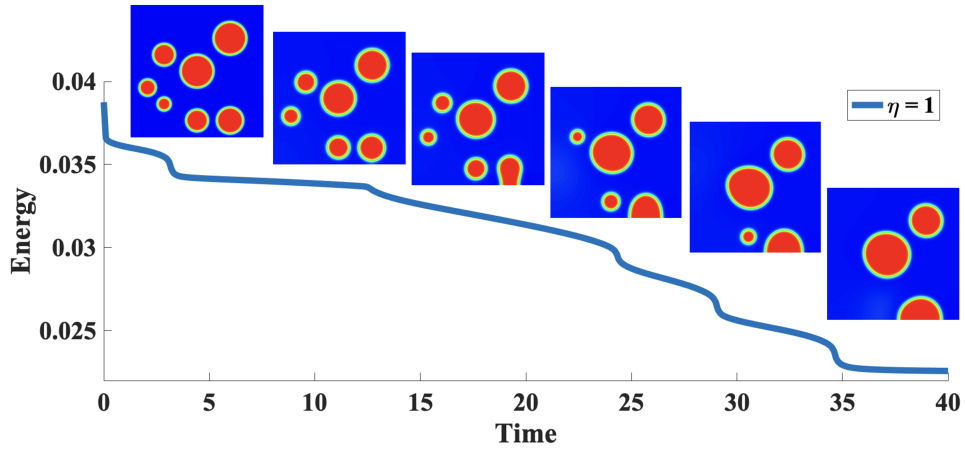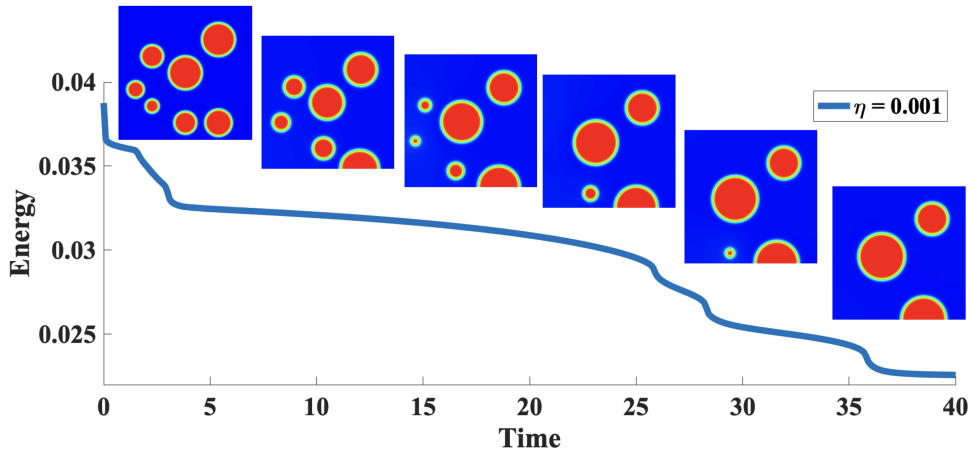Figure 5.9: Velocity field for the coarsening dynamics in Figure 5.8.
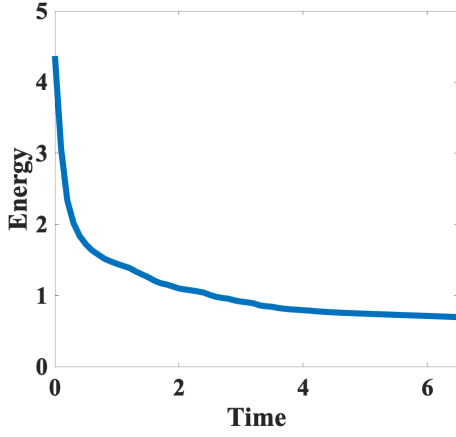
(a) Energy evolution for Figure 5.8(a)

(b) Energy evolution for Figure 5.8(b)

Figure 5.10: The time evolution of the energy for the coarsening dynamics in Figure 5.8.

(a) Energy evolution with $\eta = 1$

(b) Energy evolution with $\eta = 10^{-3}$

Figure 5.11: The time evolution of the energy under topology changes for the phase variables. In this figure, we use different viscosity parameter η with the rest parameters fixed: (a) the profiles of ϕ at $t = 0, 5, 15, 25, 30, 35$ are shown for $\eta = 1$; (b) the profiles of ϕ at $t = 0, 5, 25, 30, 35, 40$ are shown for $\eta = 10^{-3}$.

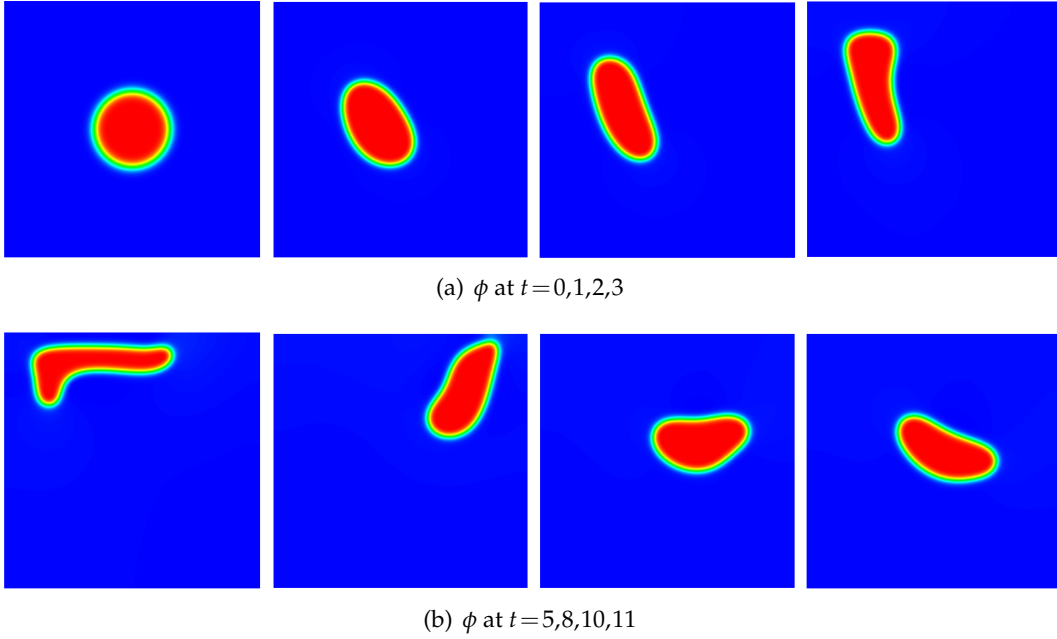(a) ϕ at $t=0,1,2,3$

(b) ϕ at $t=5,8,10,11$

Figure 5.12: drop moving in a lid-driven cavity flow. In this figure, the profiles of the phase variable ϕ are various times are shown. The drop is driven by the lid-driven cavity flow.

are summarized in Figure 5.12. We observe that our proposed numerical algorithms can accurately solve the Cahn-Hilliard-Navier-Stokes system to investigate complicated two-phase fluid flow.

6   Conclusion

How to design decoupled numerical algorithms for the well-known Cahn-Hilliard-Navier-Stokes (CHNS) system has been a long-standing problem. Many attempts are documented in published literature. So far, first-order decoupled and energy stable schemes for the CHNS system are widely available. Some recent attempts on designing second-order decoupled schemes using the SAV strategy also showing promising results. However, the schemes resulted from the SAV strategy only preserve a modified energy law, where the discrete laws are formulated using the auxiliary variables. Its connection with the discrete energy law using the original variables is not clear.

In this paper, we develop a class of second-order decoupled numerical schemes for the CHNS system that are energy stable. Our idea is based on reformulating the CHNS system into a constraint gradient flow form such that the operator splitting techniques can be utilized without destroying the discrete energy laws. With this idea, we propose several variants of decoupled and second-order numerical algorithms. All of them are shown to be energy stable. They are efficient since only problems with smaller sizes shall be solved at every time step, instead of solving a fully-coupled system. Their accuracy and effectiveness are verified numerically. Meanwhile, the idea introduced in this paper is not limited to decoupling the Navier-Stokes equation and the Cahn-Hilliard equation. It is widely applicable to a variety of hydrodynamics phase-field models. Its extensions to other coupled thermodynamic and hydrodynamic models will be pursued in our later research.

Acknowledgments

References

[1] S. M. Allen and J. W. Cahn. A microscopic theory for antiphase boundary motion and its application to antiphase domain coarsening. *Acta Metall. Mater.*, 27:1085–1095, 1979.

[2] Y. Bao and J. Kim. Multiphase image segmentation using a phase field model. *Computers and Mathematics with Applications*, 62:737–745, 2011.

[3] A. Bertozzi, S. Esedoglu, and A. Gillette. Inpainting of binary images using the Cahn-Hilliard equation. *IEEE Trans Image Process*, 16(1):285–291, 2007.

[4] F. Boyer, C. Lapuerta, S. Minjeaud, B. Piar, and M. Quintard. Cahn-Hilliard/Navier-Stokes model for the simulation of three-phase flows. *Transp Porous Med*, 82:463–483, 2010.

[5] J. W. Cahn and J. E. Hilliard. Free energy of a nonuniform system. I. interfacial free energy. *Journal of Chemical Physics*, 28:258–267, 1958.

[6] L. Chen and J. Zhao. A novel second-order linear scheme for the Cahn-Hilliard-Navier-Stokes equations. *Journal of Computational Physics*, 423:109782, 2020.

[7] L. Q. Chen. Phase-field modeling for microstructure evolution. *Annu. Rev. Mater. Res.*, 32:113–140, 2002.

[8] Y. Chen and J. Shen. Efficient, adaptive energy stable schemes for the incompressible Cahn-Hilliard Navier-Stokes phase-field models. *Journal of Computational Physics*, 308:40–56, 2016.

[9] H. Ding, P. D. M. Spelt, and C. Shu. Diffuse interface model for incompressible two-phase flows with large density ratios. *Journal of Computational Physics*, 226(2):2078–2095, 2007.

[10] Q. Du, C. Liu, R. Pyham, and X. Wang. Phase field modeling of the spontaneous curvature effect in cell membranes. *Communications on Pure and Applied Mathematics*, 4(3):537–548, 2005.

[11] D. Eyre. Unconditionally gradient stable time marching the Cahn-Hilliard equation. *Computational and mathematical models of microstructural evolution (San Francisco, CA, 1998)*, 529:39–46, 1998.

[12] W. Feng, C. Wang, S. Wise, and Z. Zhang. A second-order energy stable backward differentiation formula method for the epitaxial thin film equation with slope selection. *Numerical Methods for Partial Differential Equations*, 34(6):1975–2007, 2018.

[13] P. J. Flory. Thermodynamics of high polymer solutions. *Jounral of Chemical Physics*, 9(8):660, 1941.

[14] H. Gomez and T. J. R. Hughes. Provably unconditionally stable, second-order time-accurate, mixed variational methods for phase-field models. *Journal of Computational Physics*, 230(13):5310–5327, 2011.

[15] Y. Gong, J. Zhao, and Q. Wang. Second order fully discrete energy stable methods on staggered grids for hydrodynamic phase field models of binary viscous fluids. *SIAM J. Sci. Comput.*, 40(2):B528–B553, 2018.

[16] B. E. Griffith. An accurate and efficient method for the incompressible Navier-Stokes equations using the projection method as a preconditioner. *Journal of Computational Physics*, 228(20):7565–7595, 2009.

[17] M. Grmela and H. C. Ottinger. Dynamics and thermodynamics of complex fluids i development of a general formalism. *Phys. Rev. E*, 56(6), 1997.

[18] J. Guo, C. Wang, S. Wise, and X. Yue. An h^2 convergence of a second-order convex-splitting, finite difference scheme for the three-dimensional cahn–hilliard equation. *Commun. Math. Sci.*, 14(2):489–515, 2015.

[19] Z. Guo, P. Lin, and J. Lowengrub. A numerical method for the quasi-incompressible Cahn-Hilliard-Navier-Stokes equations for variable density flows with a discrete energy law. *Journal of Computational Physics*, 276:486–507, 2014.

[20] Z. Guo, P. Lin, J. Lowengrub, and S. Wise. Mass conservative and energy stable finite difference methods for the quasi-incompressible Navier-Stokes-Cahn-Hilliard system: primitive variable and projection-type schemes. *Computer Methods in Applied Mechanics and Engineering*, 326:144–174, 2017.

[21] D. Han and X. Wang. A second order in time uniquely solvable unconditionally stable numerical schemes for Cahn-Hilliard-Navier-Stokes equation. *Journal of Computational Physics*, 290(1):139–156, 2015.

[22] M. L. Huggins. Solutions of long chain compounds. *Jounral of Chemical Physics*, 9(5):440, 1941.

[23] D. Kay and R. Welford. Efficient numerical solution of Cahn-Hilliard-Navier-Stokes fluids in 2D. *SIAM J. Sci. Comput.*, 29(6):2241–2257, 2007.

[24] J. Kim and J. Lowengrub. Phase field modeling and simulation of three-phase flows. *Interfaces and Free Boundaries*, 7(4):435–466, 2005.

[25] J. Kou, S. Sun, and X. Wang. Linearly decoupled energy-stable numerical methods for multicomponent two-phase compressible flow. *SIAM J. Numer. Anal.*, 56(6):3219–3248, 2018.

[26] H. Lee, J. Shin, and J. Lee. First and second-order energy stable methods for the modified phase field crystal equation. *Computer Methods in Applied Mechanics and Engineering*, 321:1–17, 2017.

[27] X. Li and J. Shen. On fully decoupled MSAV schemes for the Cahn-Hilliard-Navier-Stokes model of two-phase incompressible flows. *arXiv*, page 2009.09353, 2020.

[28] C. Liu, F. Frank, C. Thiele, F. O. Alpak, S. Berg, W. Chapman, and B. Riviere. An efficient numerical algorithm for solving viscosity contrast Cahn-Hilliard-Navier-Stokes system in porous media. *J. Comput. Phys.*, 400:108948, 17, 2020.

[29] J. Lober, F. Ziebert, and I. S. Aranson. Collisions of deformable cells leads to collective migration. *Scientific Reports*, 5(9172), 2015.

[30] J. Lowengrub and L. Truskinovsky. Quasi-incompressible Cahn-Hilliard fluids and topological transitions. *Proceedings Mathematical Physical and Engineering Sciences*, 454(1978):2617–2654, 1998.

[31] Sebastian Minjeaud. An unconditionally stable uncoupled scheme for a triphasic Cahn-Hilliard Navier Stokes model. *Numerical Methods for Partial Differential Equations*, 29(2):584–618, 2013.

[32] H. C. Ottinger and M. Grmela. Dynamics and thermodynamics of complex fluids ii illustrations of a general formalism. *Phys. Rev. E*, 56(6), 1997.

[33] B. Palmieri, Y. Bresler, D. Wirtz, and M. Grant. Multiple scale model for cell migration in monolayers: Elastic mismatch between cells enhances motility. *Scientific Reports*, 5(11745), 2015.

[34] D. Shao, W. Pappel, and H. Levine. Computational model for cell morphodynamics. *Physical Review Letters*, 105, September 2010.

[35] J. Shen. Modeling and numerical approximation of two-phase incompressible flows by a phase-field approach. In *Multiscale modeling and analysis for materials simulation*, volume 22 of *Lect. Notes Ser. Inst. Math. Sci. Natl. Univ. Singap.*, pages 147–195. World Sci. Publ., Hackensack, NJ, 2012.

[36] J. Shen, C. Wang, X. Wang, and S. Wise. Second-order convex splitting schemes for gradient flows with Ehrlich-Schwoebel type energy: application to thin film epitaxy. *SIAM Journal of Numerical Analysis*, 50(1):105–125, 2012.

[37] J. Shen, J. Xu, and J. Yang. The scalar auxiliary variable (SAV) approach for gradient flows. *Journal of Computational Physics*, 353:407–416, 2018.

[38] J. Shen and X. Yang. Decoupled energy stable schems for phase field models of two phase complex fluids. *SIAM Journal of Scientific Computing*, 36(1):122–145, 2014.

[39] L. Wang and H. Yu. On efficient second order stabilized semi-implicit schemes for the Cahn-Hilliard phase-field equation. *Journal of Scientific Computing*, 77(2):1185–1209, 2018.

[40] S. Wang, R. Sekerka, A. Wheeler, B. T. Murray, S. R. Coriell, R. J. Braun, and G. B. McFadden. Thermodynamically-consistent phase-field models for solidification. *Physica D*, 69:189–200, 1993.

[41] X. Wang and Q. Du. Modeling and simulations of multi-component lipid membranes and open membranes via diffuse interface approaches. *Journal of Mathematical Biology*, 56:347–371, 2008.

[42] S. Wise. Unconditionally stable finite difference nonlinear multigrid simulation of the Cahn-Hilliard-Hele-Shaw system of equations. *Journal of Scientific Computing*, 44:38–68, 2010.

[43] S. Wise, J. Kim, and J. Lowengrub. Solving the regularized strongly anisotropic Cahn-Hilliard equation by an adaptive nonlinear multigrid method. *Journal of Computational Physics*, 226(1):414–446, 2007.

[44] X. Yang. Numerical approximations of the Navier–Stokes equation coupled with volume-conserved multi-phase-field vesicles system: Fully-decoupled, linear, unconditionally energy stable and second-order time-accurate numerical scheme. *Computer Methods in Applied Mechanics and Engineering*, 375:113600, 2021.

[45] X. Yang, J. Zhao, and Q. Wang. Numerical approximations for the molecular beam epitaxial growth model based on the invariant energy quadratization method. *Journal of Computational Physics*, 333:102–127, 2017.

[46] J. Zhao, H. Li, Q. Wang, and X. Yang. Decoupled energy stable schemes for a phase field model of three-phase incompressible viscous fluid flow. *Journal of Scientific Computing*, In Press, 2017.

[47] J. Zhao, Y. Shen, M. Happasalo, Z. J. Wang, and Q. Wang. A 3D numerical study of antimicrobial persistence in heterogeneous multi-species biofilms. *Journal of Theoretical Biology*, 392:83–98, 2016.

[48] J. Zhao, X. Yang, Y. Gong, X. Zhao, X. Yang, J. Li, and Q. Wang. A general strategy for numerical approximations of non-equilibrium models–part i thermodynamical systems. *International Journal of Numerical Analysis and Modeling*, 15(6):884–918, 2018.

[49] J. Zhao, X. Yang, J. Shen, and Q. Wang. A decoupled energy stable scheme for a hydrodynamic phase field model of mixtures of nematic liquid crystals and viscous fluids. *Journal of Computational Physics*, 305:539–556, 2016.

[50] C. Zhou, P. Yue, J. J. Feng, C. F. Ollivier-Gooch, and H. H. Hu. 3D phase-field simulations of interfacial dynamics in Newtonian and viscoelastic fluids. *Journal of Computational Physics*, 229:498–511, 2010.